

BOLU ABANT İZZET BAYSAL UNIVERSITY
THE GRADUATE SCHOOL OF NATURAL AND APPLIED
SCIENCES
DEPARTMENT OF CHEMISTRY



SYNTHESIS AND CHARACTERIZATION OF ZNO BASED
SEMICONDUCTORS WITH DOPED RARE-EARTH
METALS

MASTER OF SCIENCE

MELİKE İMAMOĞLU

BOLU, MAY 2019

APPROVAL OF THE THESIS

SYNTHESIS AND CHARACTERIZATION OF ZnO BASED SEMICONDUCTORS WITH DOPED RARE-EARTH METALS submitted by **MELİKE İMAMOĞLU** in partial fulfillment of the requirements for the degree of **Master of Science** in **Department of Chemistry, The Graduate School of Natural and Applied Sciences of BOLU ABANT İZZET BAYSAL UNIVERSITY** in 24/05/2019 by,

Examining Committee Members

Signature

Supervisor
Assoc. Prof. Dr. Sevim DEMİRÖZÜ ŞENOL
BOLU ABANT İZZET BAYSAL
UNIVERSITY

.....

Member
Asst. Prof. Dr. Erhan BUDAK
BOLU ABANT İZZET BAYSAL
UNIVERSITY

.....


Member
Asst. Prof. Dr. Elif AŞIKUZUN
KASTAMONU UNIVERSITY

.....


Graduation Date :

Prof. Dr. Ömer ÖZYURT



Director of Graduate School of Natural and Applied Sciences



To my family

DECLARATION

I hereby declare that all information in this document has been obtained and presented in accordance with academic rules and ethical conduct. I also declare that, as required by these rules and conduct, I have fully cited and referenced all material and results that are not original to this work.

MELİKE İMAMOĞLU



ABSTRACT

SYNTHESIS AND CHARACTERIZATION OF ZNO BASED SEMICONDUCTORS WITH DOPED RARE-EARTH METALS MSC THESIS

MELİKE İMAMOĞLU

BOLU ABANT İZZET BAYSAL UNIVERSITY GRADUATE SCHOOL OF
NATURAL AND APPLIED SCIENCES
DEPARTMENT OF CHEMISTRY

(SUPERVISOR: ASSOC.PROF.DR. SEVİM DEMİROZU ŞENOL)

BOLU, MAY 2019

This thesis consist of synthesis and characterization of Erbium (Er) and Praseodymium (Pr) from rare-earth metals doped zinc oxide (ZnO) thin film and bulk materials. RF sputter and hydrothermal method were used for synthesizing the targeted materials.

First chapter of this thesis, polyethylene terephthalate and glass substrates were coated with ZnO target before the synthesis. Then ZnO based semiconducting thin film materials were produced while doping of different Er concentrations ($Zn_{1-x}Er_xO$) ($x=0.01, 0.03, 0.05, 0.07, 0.09$) on PET and glass substrates by hydrothermal method. All that the obtained substances were determined as hexagonal wurtzite structure.

In the second chapter, bottom of ZnO thin film semiconducting materials were produced of doping Pr on glass substrates ($Zn_{1-x}Pr_xO$) ($x=0.01, 0.02, 0.03, 0.04, 0.05$). That obtained semiconductor materials were determined as hexagonal crystal structure and calculated the cell parameters by investigation of X-ray powder diffraction which the cell parameters $a=3.214$ $c=5.156$ $Zn_{0.99}Pr_{0.01}O$, $a=3.220$ $c=5.164$ $Zn_{0.98}Pr_{0.02}O$, $a=3.218$ $c=5.162$ $Zn_{0.97}Pr_{0.03}O$, $a=3.219$ $c=5.162$ $Zn_{0.96}Pr_{0.04}O$, $a=3.212$ $c=5.152$ $Zn_{0.95}Pr_{0.05}O$.

Finally, in the last section, $Zn_{1-x}Ln_xO$ type ($x=0.01, 0.02, 0.03, 0.04, 0.05$) semiconductor bulk materials were synthesized using Ln: Er and Pr from rare-earth metals by hydrothermal method. Those semiconductor bulk materials that obtained were determined as hexagonal wurtzite structure.

Structure, morphology, and optical properties of obtained materials were investigated by X-ray powder diffraction (XRD), scanning electron microscopy (SEM)-energy dispersive spectroscopy (EDS), ultraviolet diffuse reflectance spectra (UV-DRS).

KEYWORDS: Zinc oxide, Rare-earth metal, Hydrothermal method, XRD, SEM, UV-VIS

ÖZET

**ZNO TABANLI YARIİLETKENLERİN NADİR TOPRAK KATKILI
METALLER İLE SENTEZLENMESİ VE KARAKTERİZASYONU
YÜKSEK LİSANS TEZİ
MELİKE İMAMOĞLU
BOLU ABANT İZZET BAYSAL ÜNİVERSİTESİ
FEN BİLİMLERİ ENSTİTÜSÜ
KİMYA ANABİLİM DALI
(TEZ DANIŞMANI: DOÇ. DR. SEVİM DEMİRÖZÜ ŞENOL)**

Bolu, MAYIS - 2019

Bu tez, nadir toprak metallere Erbiyum (Er) ve praseodim (Pr) katkıları çinko oksit (ZnO) tabanlı ince film ve toz yarıiletken malzemelerin sentezi ve karakterizasyonunu kapsamaktadır. Hedeflenen malzemelerin sentezlenmesinde RF sputter ile hidrotermal yöntem kullanılmıştır.

Bu tezin ilk bölümünde sentez öncesinde PET ve cam altlıklar RF sputterda ZnO target ile kaplanmıştır. Daha sonra PET ve cam altlık üzerinde farklı konsantrasyonlar da Erbiyum katkıları ile $(Zn_{1-x}Er_xO)$ ($x= 0.01, 0.03, 0.05, 0.07, 0.09$) çinko oksit tabanlı yarı iletken ince film malzemeler hidrotermal yöntemle sentezlenmiştir. Oluşan tüm malzemelerin wurtzite heksagonal yapıda olduğu saptanmıştır.

İkinci bölüm de cam altlık üzerine Praseodim katkıları ile $(Zn_{1-x}Pr_xO)$ ($x=0.01, 0.02, 0.03, 0.04, 0.05$) ZnO tabanlı ince film yarıiletkenleri üretilmiştir. Elde edilen yarıiletken malzemelerin X-ışını toz kırınımı verilerinin incelenmesiyle heksagonal Kristal yapıda olduğu tespit edilmiş olup birim hücre parametreleri $a=3.214$ $c=5.156$ $Zn_{0.99}Pr_{0.01}O$, $a=3.220$ $c=5.164$ $Zn_{0.98}Pr_{0.02}O$, $a=3.218$ $c=5.162$ $Zn_{0.97}Pr_{0.03}O$, $a=3.219$ $c=5.162$ $Zn_{0.96}Pr_{0.04}O$, $a=3.212$ $c=5.152$ $Zn_{0.95}Pr_{0.05}O$ olarak hesaplanmıştır.

Bu çalışmanın son bölümünde ise, nadir toprak metallere Ln: Er ve Pr kullanılarak $Zn_{1-x}Ln_xO$ ($x= 0.01, 0.02, 0.03, 0.04, 0.05$) tipinde ki yarıiletken toz malzemeler hidrotermal yöntemle sentezlenmiştir. Elde edilen yarıiletken toz malzemelerin wurtzite heksagonal yapıda olduğu belirlenmiştir.

Üretilen malzemelerin karakterizasyonu X-ışını toz kırınımı (XRD), taramalı electron mikroskopu (SEM)-elektron dağılım spektroskopisi (EDS) ve optik özellikleri ise ultraviyole ayrıntılı yansıma-dağılımlı (UV-DRS) yöntemleri ile incelenmiştir.

ANAHTAR KELİMELEER: Çinko oksit, Nadir-toprak metali, hidrotermal metod, XRD, SEM, UV-VIS

TABLE OF CONTENTS

	<u>Page</u>
ABSTRACT	v
ÖZET	vi
TABLE OF CONTENTS	vi
LIST OF TABLES	ix
LIST OF FIGURES	x
LIST OF ABBREVIATIONS AND SYMBOLS	xiii
1. INTRODUCTION	1
1.1 Zinc oxide.....	1
1.1.1 History of Zinc oxide	1
1.1.2 General properties of ZnO	3
1.1.3 ZnO in Industry	5
1.1.4 Doping of ZnO Nanostructures	7
1.1.5 Synthesis Methods	9
2. AIM AND SCOPE OF THE STUDY	10
3. MATERIALS AND METHODS	11
3.1 Chemicals	11
3.2 Characterization.....	12
3.2.1 X-ray Diffraction (XRD).....	12
3.2.2 Scanning electron microscope (SEM) and energy dispersive study(EDS).....	12
3.2.3 Chamber Furnaces.....	13
3.2.4 UV-VIS Diffuse Reflectance Spectra (UV-VIS-DRS).....	14
3.2.5 RF Magnetron Sputtering.....	15
3.3 Experimental Procedure	16
3.4 Preparation of ZnO films on PET and glass.....	16
3.4.2 Preparation of Zn _{1-x} Er _x O nanoparticles by hydrothermal method (X=0.01, 0.03, 0.05, 0.07, 0.09).....	19
3.4.3 Preparation of Zn _{1-x} Pr _x O nanoparticles by hydrothermal method (X=0.01,0.02,0.03,0.04,0.05).....	19
4. RESULT AND DISCUSSION	20
4.1 ZnO films on glass substrates.....	20
4.1.1 X-ray Diffraction (XRD) study.....	20
4.2 Zn _{1-x} Er _x O films (x=0.03,0.05,0.07,0.09) on glass substrates	21
4.2.1 XRD study.....	21
4.2.2 Scanning electron microscopy SEM and energy dispersive X-ray EDX study	24
4.2.3 Optical properties	27
4.3 Zn _{1-x} Er _x O films (x=0.03, 0.05, 0.07, 0.09) on PET substrate.....	29

4.3.1 XRD studies	29
4.3.2 SEM-EDS Studies.....	31
4.3.3 Optical Properties.....	34
4.4 Zn _{1-x} Pr _x O films (x=0.01, 0.02, 0.03, 0.04, 0.05) on glass substrate.....	36
4.4.1 XRD Study	36
4.4.2 SEM-EDS.....	37
4.4.3 Optical Properties.....	41
4.5 Preparation of Zn _{1-x} Er _x O nanoparticles by hydrothermal method (x= 0.03, 0.05, 0.07, 0.09)	43
4.5.1 XRD Study	43
4.5.2 SEM-EDS Study	44
4.5.3 Optical Properties.....	47
4.6 Preparation of Zn _{1-x} Pr _x O nanoparticles by hydrothermal method (x=0.01, 0.02, 0.03, 0.04, 0.05)	49
4.6.1 XRD Study	49
4.6.2 SEM-EDS Study	51
4.6.3 Optical Properties.....	56
5. CONCLUSIONS	59
6. REFERENCES.....	61
7. APPENDICES	66
7.1 Appendix A XRD data of samples	66
8. CURRICULUMVITAE.....	68

LIST OF TABLES

	<u>Page</u>
Table 1.1. General properties of ZnO.....	1
Table 4.1. Concentration-dependent average particle sizes, lattice parameters, atomic packing factor(c/a), crystal lattice distortion degree and volume of the unit cell $Zn_{1-x}Er_xO$ thin films on glass substrate.....	23
Table 4.2. Cell parameters, crystallite sizes, bond lengths, crystal lattice distortion degree and volume of unit cell of $Zn_{1-x}Er_xO$ thin films on PET substrate.....	30
Table 4.3. Cell parameter, atomic packing factor (c/a), particle sizes, bond length, crystal lattice distortion degree, and volume of unit cell $Zn_{1-x}Pr_xO$ thin films on glass substrate.	37
Table 4.4. Cell parameters, atomic packing factor, average particle size, crystal lattice distortion degree, bond length and volume of the cell $Zn_{1-x}Er_xO$ nanoparticles.....	44
Table 4.5 Cell parameters, atomic packing factor, average particle size, bond length, crystal lattice distortion degree and volume of the unit cell $Zn_{1-x}Pr_xO$ nanoparticles.....	51
Table A.1. 2θ , d and hkl values of $Zn_{1-x}Er_xO$ (x= 0.03, 0.05, 0.07, 0.09) thin films on glass substrates.....	66
Table A.2. The 2θ , d, and hkl values of $Zn_{1-x}Er_xO$ (x=0.03, 0.05, 0.07, 0.09) films on PET substrate	66
Table A.3. The 2θ , d and hkl values of $Zn_{1-x}Pr_xO$ films on glass substrate (x=0.01, 0.02, 0.03, 0.04, 0.05).....	67
Table A.4. The 2θ , d and hkl values of $Zn_{1-x}Er_xO$ nanoparticles (x=0.03, 0.05, 0.07, 0.09).....	67
Table A.5. The 2θ , d and hkl values of $Zn_{1-x}Pr_xO$ nanoparticles (x=0.01, 0.02, 0.03, 0.04, 0.05).....	67

LIST OF FIGURES

	<u>Page</u>
Figure 1.1. Zinc oxide powder	1
Figure 1.2. The hexagonal wurtzite structure of Zinc oxide.....	3
Figure 1.3. n-type and p-type semiconductor.....	4
Figure 1.4. Energy band gap diagram	4
Figure 1.5. Examples of semiconductors	5
Figure 1.6. Global marketing of ZnO.....	7
Figure 1.7. Types of application of ZnO.....	7
Figure 3.8. Rigaku MultiFlex 2kW Diffractometer	12
Figure 3.9. Jeol model-JSM 6390 LV-;Scanning Electron Microscope.....	13
Figure 3.10. The PROTHERM FURNACE Chamber Furnace-PLF Series (150/5).....	14
Figure 3.11. Shimadzu UV-VIS 2450 diffuse reflectance	15
Figure 3.12. Plasmalab 80 Plus RF sputter	16
Figure 3.13. Teflon-lined autoclave	17
Figure 3.14. Er-doped glass substrate	18
Figure 4.15. XRD patterns of ZnO film on glass substrate.....	20
Figure 4.16. a) XRD patterns of $Zn_{1-x}Er_xO$ ($x = 0.03, 0.05, 0.07, 0.09$) on glass substrate b) $Zn_{0.93}Er_{0.07}O$ XRD profile fitting from Rietveld analysis.....	23
Figure 4.17. SEM images of the $Zn_{1-x}Er_xO$ ($x=0.03, 0.05, 0.07, 0.09$) on glass substrates respectively with 10 μm magnification 5 μm magnification.....	25
Figure 4.18. EDS image of the $Zn_{1-x}Er_xO$ films a) $Zn_{0.97}Er_{0.03}O$ b) $Zn_{0.95}Er_{0.05}O$ c) $Zn_{0.93}Er_{0.07}O$ d) $Zn_{0.91}Er_{0.09}O$ respectively	29
Figure 4.19. Optical transmittance spectra of $Zn_{1-x}Er_xO$ film ($x = 0.01, 0.03, 0.05, 0.07, 0.09$) on glass substrate.....	31
Figure 4.20. The plots of $(\alpha h\nu)^2$ versus photon energy ($h\nu$) of $Zn_{1-x}Er_xO$ films ($x=0.01, 0.03, 0.05, 0.07, 0.09$) on glass substrate.....	32
Figure 4.21. a) XRD patterns of $Zn_{1-x}Er_xO$ ($x=0.03, 0.05, 0.07, 0.09$) on PET substrate b) the XRD profile fitting from the Rietveld analysis of $Zn_{0.91}Er_{0.09}O$	34
Figure 4.22. SEM images of the $Zn_{1-x}Er_xO$ ($x = 0.03, 0.05, 0.07, 0.09$) on glass substrates respectively with 10 μm magnification and 5 μm magnification.....	36
Figure 4.23. EDX image of the $Zn_{1-x}Er_xO$ films ($x=0.03, 0.05, 0.07, 0.09$) on PET substrate a) $Zn_{0.97}Er_{0.03}O$ b) $Zn_{0.95}Er_{0.05}O$ c) $Zn_{0.93}Er_{0.07}O$ d) $Zn_{0.91}Er_{0.09}O$ respectively	38
Figure 4.24. Optical absorbance spectra of $Zn_{1-x}Er_xO$ films ($x = 0.03, 0.05, 0.07,$ 0.09) on PET substrate	39
Figure 4.25. The plots of $(\alpha h\nu)^2$ versus photon energy ($h\nu$) of $Zn_{1-x}Er_xO$ films ($x = 0.03, 0.05, 0.07, 0.09$) on PET substrate.....	40
Figure 4.26. a) XRD patterns of $Zn_{1-x}Pr_xO$ ($x=0.01, 0.02, 0.03, 0.04, 0.04$) on glass substrate b) the XRD profile fitting from Rietveld analysis of $Zn_{0.97}Pr_{0.03}O$	41

Figure 4.27. SEM images of 1%, 2%, 3%, 4%, 5% $Zn_{1-x}Pr_xO$ films a) $Zn_{0.99}Pr_{0.01}O$ b) $Zn_{0.98}Pr_{0.02}O$ c) $Zn_{0.97}Pr_{0.03}O$ d) $Zn_{0.96}Pr_{0.04}O$ e) $Zn_{0.95}Pr_{0.05}O$ respectively with 10 μm magnification and 5 μm magnification.....	38
Figure 4.28. EDX image of the $Zn_{1-x}Pr_xO$ nanoparticles a) $Zn_{0.99}Pr_{0.01}O$ b) $Zn_{0.98}Pr_{0.02}O$ c) $Zn_{0.97}Pr_{0.03}O$ d) $Zn_{0.96}Pr_{0.04}O$ e) $Zn_{0.95}Pr_{0.05}O$ respectively.....	41
Figure 4.29. Absorbance spectra of $Zn_{1-x}Pr_xO$ films ($x= 0.01, 0.02, 0.03, 0.04,$ 0.05) on glass substrate	42
Figure 4.30. The plots of $(\alpha hv)^2$ versus photon energy ($h\nu$) of $Zn_{1-x}Pr_xO$ films ($x= 0.01, 0.02, 0.03, 0.04, 0.05$) on glass substrate.....	42
Figure 4.31. a) XRD patterns of $Zn_{1-x}Er_xO$ nanoparticles ($x= 0.03, 0.05, 0.07,$ 0.09) b) the XRD profile fitting from Rietveld analysis of $Zn_{0.93}Er_{0.07}O$	44
Figure 4.32. SEM images of the $Zn_{1-x}Er_xO$ ($x=0.03, 0.05, 0.07, 0.09$) nanoparticles respectively with 10 μm and 5 μm magnification	50
Figure 4.33. EDX images of $Zn_{1-x}Er_xO$ nanoparticles a) $Zn_{0.97}Er_{0.03}O$ b) $Zn_{0.95}Er_{0.05}O$ c) $Zn_{0.93}Er_{0.07}O$ d) $Zn_{0.91}Er_{0.09}O$ respectively.....	47
Figure 4.34. The reflectance spectra of the $Zn_{1-x}Er_xO$ ($x=0.01, 0.03, 0.05, 0.07,$ 0.09) nanoparticles	48
Figure 4.35. The plots of $dR/d\lambda$ as a function of wavelength for the $Zn_{1-x}Er_xO$ ($x=0.01, 0.03, 0.05, 0.07, 0.09$) nanoparticles.....	49
Figure 4.36. a) XRD patterns of $Zn_{1-x}Pr_xO$ ($x=0.01, 0.02, 0.03, 0.04, 0.05$) nanoparticles b) the XRD profile fitting from Rietveld analysis of $Zn_{0.98}Pr_{0.02}O$	50
Figure 4.37. SEM images of 1%, 2%, 3%, 4%, 5% $Zn_{1-x}Pr_xO$ nanoparticles a) $Zn_{0.99}Pr_{0.01}O$ b) $Zn_{0.98}Pr_{0.02}O$ c) $Zn_{0.97}Pr_{0.03}O$ d) $Zn_{0.96}Pr_{0.04}O$ e) $Zn_{0.95}Pr_{0.05}O$ respectively with 10 μm magnification and 5 μm magnification.....	53
Figure 4.38. EDX image of the $Zn_{1-x}Pr_xO$ nanoparticles a) $Zn_{0.99}Pr_{0.01}O$ b) $Zn_{0.98}Pr_{0.02}O$ c) $Zn_{0.97}Pr_{0.03}O$ d) $Zn_{0.96}Pr_{0.04}O$ e) $Zn_{0.95}Pr_{0.05}O$ respectively.....	56
Figure 4.39. The reflectance of the $Zn_{1-x}Pr_xO$ ($x=0.01, 0.02, 0.03, 0.04, 0.05$) nanoparticles.....	62
Figure 4.40. The plots of $dR/d\lambda$ as a function of wavelength for the $Zn_{1-x}Pr_xO$ ($x=0.01, 0.02, 0.03, 0.04, 0.05$) nanoparticles.....	58

LIST OF ABBREVIATIONS AND SYMBOLS

Al	:Aluminium
Er	: Erbium
EDS	: Energy Dispersive Spectroscopy
FTIR	: Fourier Transform Infrared Spectroscopy
ITO	: Indium tin oxide
PET	: Polyethylene terephthalate
Pr	: Praseodymium
RF	: Radio Frequency
SEM	: Scanning Electron Microscopy
UV-DRS	: Ultraviolet Diffuse Reflectance Spectroscopy
ZnO	: Zinc Oxide
XRD	: X-Ray Diffractometer

ACKNOWLEDGEMENTS

I would like to thank my advisor, Doç.Dr.Sevim DEMİRÖZÜ ŞENOL for their guidance, advice, and encouragements throughout the research.

I would like to thank my family for all their support and faith during my education.



1. INTRODUCTION

1.1 Zinc oxide

1.1.1 History of Zinc oxide

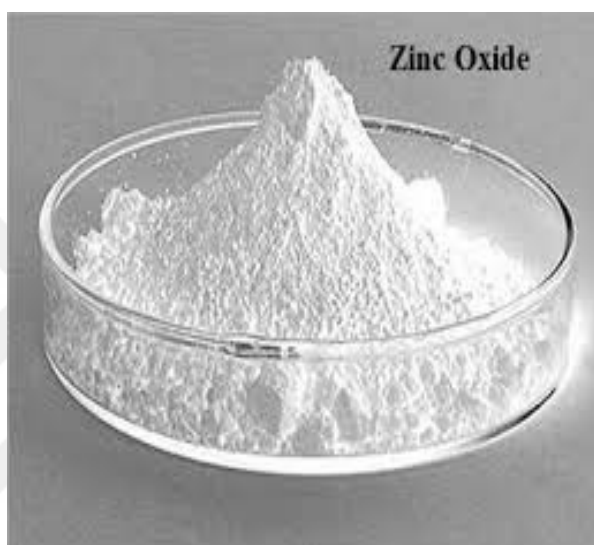


Figure 1.1. Zinc oxide powder

Zinc oxide is highly significant zinc compounds. ZnO can be prepared in high purity and in a variety of crystal shapes and sizes by burning zinc vapor in air. Zinc is the most ample element in the Earth. Zinc is mostly exist in Australia, Asia (The editors of Encyclopaedia Britannica 2019).



Table 1.1. General properties of ZnO

Formula	ZnO
Molar mass	81.408 g/mol
Melting point	-1975 C
Boiling point	-2360 C
Density	5.606 g/cm ³

ZnO is a white powder chemical that is nonsoluble in water but soluble in acids and bases. It has wurtzite structure Zinc oxide is known as Zincite. So that most

ZnO commercially is synthetic. It was also used in ancient times. Many people have used zinc oxide for making paints, oils, and acrylic paints (Faloon n.d.).

Since the 12th century the Indians have known zinc and zinc ore, and began to make brass. Zinc smelting technology introduced in China in seventeenth century. 1743, Bristol Britain established the first zinc smelting plant in Europe. In 1746, A German chemist discovered zinc in that pure metallic form. It was settled the periodic table as an element by Antonie Lavoisier in 1789.

Other important use of zinc oxide is coating, called zinc white. In 1834, Zinc as became the Chinese watercolor paint for the first time. In 1845, LeClaire began to manufacture pigment of zinc white oil painting on a large area in Paris, to 1850 zinc white popular throughout Europe. During the end 1890's and early 1900's some painters used zinc oxide as a ground for oil paintings (Zinc oxide | 1314-13-2 n.d.).

The first use of ZnO for electronic applications was in build own radio set in the 1920's. A Schottky barrier was created by contacting a ZnO crystal with a copper wire, providing the correction needed to convert the AC radio waves to DC signals. The light emission from ZnO was making splash after some initial work in Germany in the 1930's. In 1935, first electron diffraction data appeared, after three year later first scanning electron microscope display taken of ZnO crystal.

In the 20th century ZnO used in rubber industry and additives of copy paper. From those years, synthesis of ZnO thin films has been an efficient area because of their applications as sensor, transducers, and catalysts. ZnO is a key technological material. The lack of a center of symmetry in wurtzite, combined with large electromechanical coupling, it is useful for as a sensor, converter, and energy generator in strong piezoelectric and pyroelectric properties (Z. L. Wang 2004).

1.1.2 General properties of ZnO

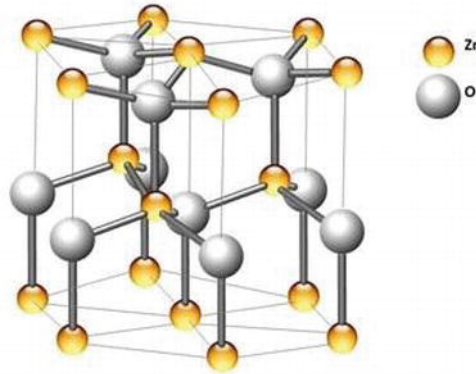


Figure 1.2. The hexagonal wurtzite structure of Zinc oxide.

ZnO has own three crystal structures: wurtzite, zinc blende, and rock salt. However, wurtzite structure with hexagonal lattice ($a=0.325$ nm, $c=0.521$ nm) is most stable at ambient conditions that every zinc atom is tetrahedrally coordinated with four oxygen atoms. Electron configuration of zinc oxide $1s^2, 2s^2, 2p^6, 3s^2, 3p^6, 3d^{10}, 4s^2$ that zinc has 30 atomic number. Thus the outer shell electrons are in the 3d&4s orbitals. The d orbitals are totally filled up. The highest occupied molecular orbital (HOMO) in the valence band is made up of d orbitals. The lowest occupied molecular orbital (LUMO) is filled with s and p hybridized orbitals (Cagardová and Lukeš 2017). So that there is a difference in the nature of HOMO and LUMO (dissimilar parity) that retards the return of the excited electron to the valence bond.

ZnO is the fundamental catalyst due to non-toxic feature, belongs to the group II-VI semiconductors, n-type and has large band-gap of 3.37 eV this provides that its most versatile material, hold a huge excitation binding energy of 60 meV at room temperature, high chemical stability, and low dielectric constant (M. Wang, Zhao, and Liu 2015).

Materials can be divided into three categories: conductors, insulators, and semiconductors. The difference in their band gaps explain the general properties of this material. The band gap is meaning energy difference between the valence band and the conduction band that is electron not exist. Conductors have not include band gap, insulators have a large band gap. Although semiconductors involve a small band

gap and the flow of electrons, electron holes can be controlled by adding impurities to the material e.g by doping. These adding impurities that produce electrons are called n-type semiconductors (n is negative), and some impurities that create a deficiency of electrons are called p-type (p is positive) semiconductors (Carl R.(Rod) Nave 2017).

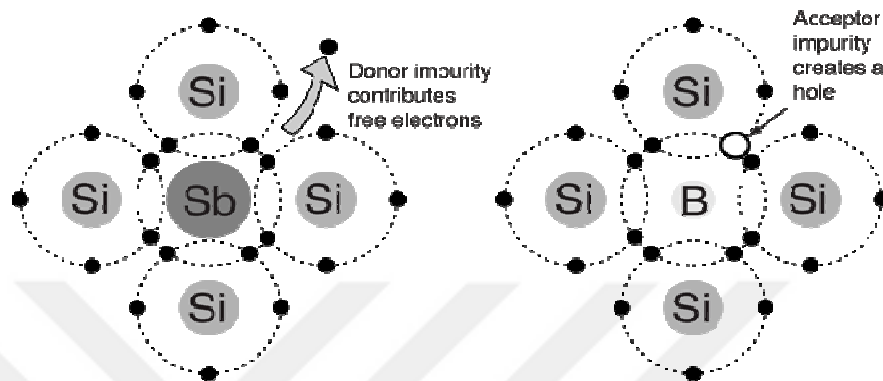


Figure 1.3. n-type and p-type semiconductor.

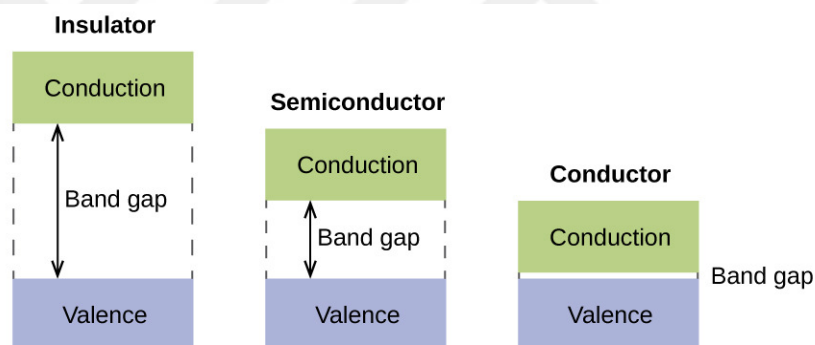


Figure 1.4. Energy band gap diagram

They are neither a conductor nor an insulator that semiconducting materials (including group IV elements Si and Ge) mostly silicon, and gallium arsenide (Pearsonhighered 2013). Semiconductors play a big role in various kind of technology which are diodes, transistors, and integrated circuits, our telephones, computers, and in cars.

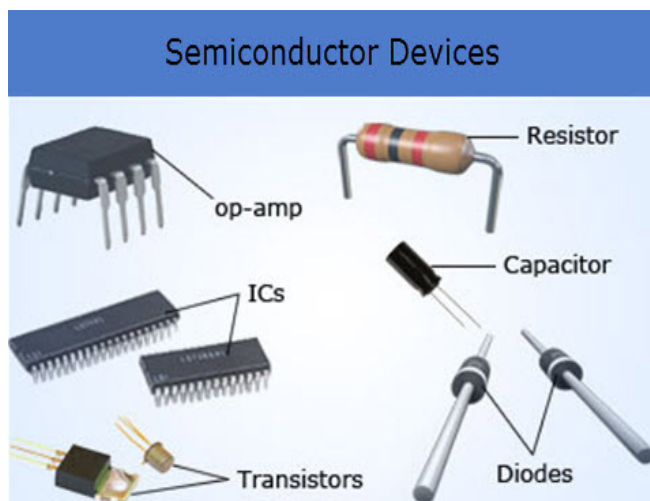


Figure 1.5 Examples of semiconductors

So this various specialties make ZnO excellent for using the photodetector, solar cells, gas sensors, light emitting diodes (S. D. Senol 2016). In addition, ZnO is an economical and environment-friendly having low price, high electrical conductivity, splendid mechanical-electrical characteristics (Agrawal et al. 2017). As such ZnO is very old discovered material. To improve these properties it is important to adjust the productivity of ZnO by doping. Such as rare-earth elements achieve that procedure.

1.1.3 ZnO in Industry

Zinc oxide is mainly used in various applications such as in pharmaceutical, cosmetic, food, rubber, painting, ceramic, and glass industries.

FOOD

ZnO is used as food additive by the US food and drug administration, zinc is essential trace element. Zinc oxide nanoparticles have been contained in polymeric structures in order that ensure antimicrobial condition to the packaging substances.

RUBBER

Rubber products performed the largest market for zinc oxide. ZnO is quite used in rubber industry due to as an activator for vulcanization of rubber. So ZnO adds strength to rubber compounds and provides resistance against heat.

Another common use, ZnO assists the treat of concrete and improves the water resistance.

COSMETICS

ZnO contribute to many hair and skin care cosmetics compounds. Also, it has antibacterial and deodorizing properties. So used in medicinal applications such as baby powder, creams, and sunscreen lotions. Protect the skin by harmful ultraviolet rays.

GLASS

Zinc oxide nanoparticles included in various materials including glass, low-density polyethylene, polypropylene, paper (Oxide et al. 2016). In glass, ZnO tends to increase the chemical durability. Used in phosphate glasses, chemically resistant glass wares and certain fiberglass compositions. ZnO minimalizes the coefficient of thermal expansion, imparts high brilliance, luster, and high stability against impairment under stress (Kolodziejczak-Radzimska and Jesionowski 2014).

PAINTS

ZnO is an significant material of durables and protective paints. Provide the protection the paint from mildew, enhances resistance to abrasion (Lang et al. 2016).

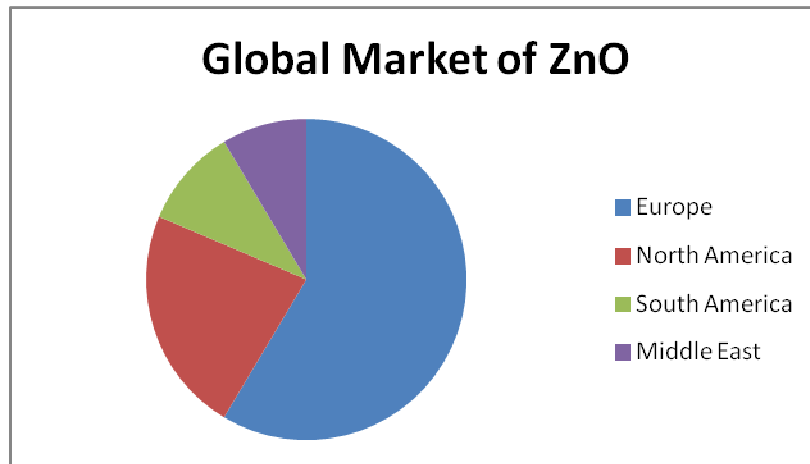


Figure 1.6 Global marketing of ZnO

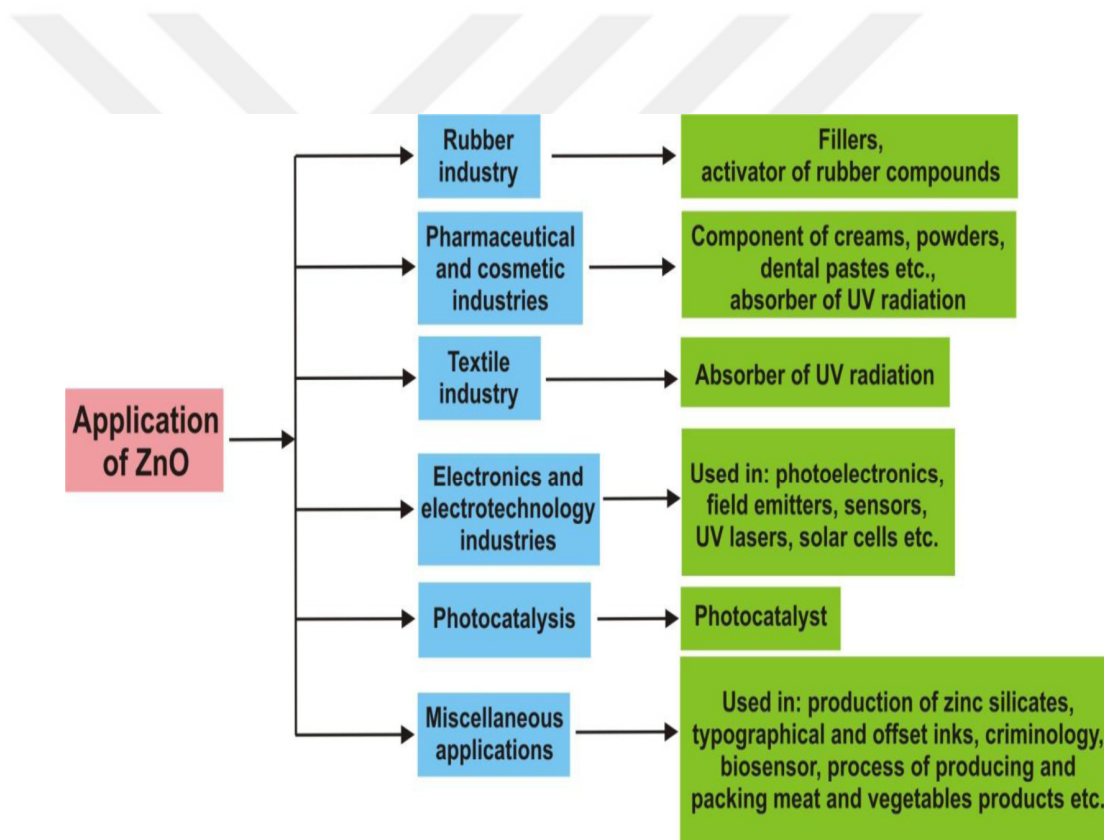


Figure 1.7 Types of application of ZnO

1.1.4 Doping of ZnO Nanostructures

Doping of semiconducting material is the fundamental method for controlling properties like bandgap and electrical conductivity (Ebnesajjad and Fluoroplastics 2003). ZnO is wide bandgap semiconductor, high thermal stability, environmental

friendly. These specialties make the ZnO is proper host material for doping. Nowadays, many researchers had been studied rare-earth doped ZnO films. Rare-earth elements doping (Eu, Er, etc.) can cause the variation of luminescence properties of ZnO because of the transition between 4f –shells (Üzar 2018). ZnO doped nanorods noted as a proper nominee as conductors with high transparency in the visible light. The reason of this function the 4f shells surrounded by totally filled 5s and 5p shells. Thus provides very powerful emission lines in the ultraviolet and visible regions (Kaur et al. 2018). Rare-earth (RE) ion doped ZnO materials are expected to be inventive materials because of that have efficient modulate the emission power due to their proper optical properties(Fan, Lu, and Li 2017). There are 17 elements in lanthanide group but still, rare-earth doped ZnO are not common. ZnO is the proper matrix material to host the Er ions. Er-doped ZnO materials are excellent for using in optical applications because they can emit the luminescence including 1.54 μm infrared emission. Also, Er exhibit sharp emission lines and encourage to 4f-4f transition of Er by changing the native surrounding in ZnO (Lang et al. 2016). According to Bhatia (Bhatia, Verma, and Bedi 2016). Er has great effect like morphological, band gap and photocatalytic activity on ZnO nanostructures.

Rare-earth metals are technologically important materials in optoelectronic devices. Pr⁺³ has unique optical properties that have been widely studied especially in laser applications. Navas and coworkers reported that the Pr-doped nanofilms have splendid optical transparency, show UV and visible emission (Sreedharan et al. 2016). Also, Pr-ZnO ceramics have considered useful material for varistor applications (Lop et al. 2015). For instance, praseodymium doped zinc oxide films have not been worked extensively. Matarangolo reported that Pr-doped ZnO photocatalyst established the best photocatalytic performance for discoloration under UV light (Anker 2012). In our work, we investigated these properties.

Polyethylene terephthalate (PET) is a thermoplastic polymer and the application of ZnO on PET has great attention because of low cost, flexibility, lightweight and transparency. Also, Indium tin oxide coated glass substrate commonly used materials (Jiang et al. 2004). In this study, we synthesized Er and Pr doped ZnO nanorods by hydrothermal method on ITO coated glass substrate and PET substrate.

1.1.5 Synthesis Methods

So far, multiple chemical and physical deposition techniques have been performed to produce ZnO nanoparticles, nanobelts, nanowires, nanotubes. These methods are sol-gel, thermal evaporation, wet chemical, spray-pyrolysis, vapor deposition, electrochemical deposition, hydrothermal, pulse laser deposition, molecular and microemulsion environment method. All methods have advantages and disadvantages (Zamiri et al. 2014). For example, pulse laser deposition and vapor deposition techniques involve disadvantages like high price, difficult reaction conditions, and much more impurity. On the other way, sol-gel and especially spray pyrolysis have advantages for instance high purity, homogeneous and easy to control the conditions.

Why hydrothermal method? Hydrothermal method ensures lots of properties that is low cost, effective and easy to control the process at low temperature. Main reason to choose this method that ZnO doped semiconducting materials rarely exist in the literature. Hydrothermal method on the contrary other conventional and nonconventional methods provide many advantages (Heo et al. 2014). All forms of inorganic materials meaning bulks, single crystals, fibers, polymers, and ceramic materials can be accelerate by hydrothermal method. Also, this method is safe for environmental. Hydrothermal method ensures energy-saving at low temperatures, recyclable waste. On this method does not need to use of additional processing of the product (calcination and grinding) that make it is simple. This is fast technique that can produce high product yields (McLeod 2012). For instance, hydrothermal reaction can take in a few days while solid-state reactions taking much more time. The studies of physical properties of doping or undoing of ZnO thin films were limited availability in the literature (Sakthivel et al. 2017), (Venkatachalam et al. 2013), (Zou et al. 2014). For example, the structural, morphological and optical properties were investigated of Al-doped films that obtained using different starting material by hydrothermal method. Additionally, the benefit of these method morphologies of obtained Al-doped ZnO thin films can easily bring under control while using various surface-active substances.

2. AIM AND SCOPE OF THE STUDY

ZnO (zinc oxide) that include Zn and O atoms has hexagonal wurtzite structure. Due to the 3.37 eV bandgap and strong binding energy, ZnO is one of the most important structure among the semiconductors (Yu et al. 2014). These properties provide lots of use in the area such as optical/sonics wave devices, chemical sensor, solar cells, flat panels diodes, conductivity electrodes, etc. (Chen et al. 2013). In recent years, studies on rare earth doped semiconductor samples have concentrated on the optical properties that reveal that the potential for it use in optoelectronic devices (Lin et al. 2010), (Background et al. 2004). Especially, rare earth metal doped semiconductor ZnO structures constitute possibility of alternative usage for flat panel display based produced using ZnO. Therefore, synthesis and construction of new rare-earth metal doped semiconductor materials are very important materials. These materials to be obtained can be used as advanced technology material with their common usage characteristics. Thereby, the aim of this study can be summarize in three part:

- 1) The synthesis of rare-earth metals (Er, Pr) doping of ZnO thin films materials on PET and glass substrates
- 2) Synthesis of rare-earth metals (Er, Pr) doping of ZnO bulk materials by hydrothermal method
- 3) The obtained substances will be characterize separately, the determination of crystal structure by XRD technique, the surface morphology by SEM-EDX and the optical properties by diffuse reflectance (detailed reflection-dispersed) UV-DRS.

3. MATERIALS AND METHODS

3.1 Chemicals

The following chemicals are used in the synthesis of the products:

Erbium (III) acetate tetrahydrate ($\text{Er}(\text{CH}_3\text{CO}_2)_2 \cdot 4\text{H}_2\text{O}$) (%99.9 Alfa Aesar),

Zinc acetate dihydrate ($\text{Zn}(\text{CH}_3\text{COO})_2 \cdot 2\text{H}_2\text{O}$)(Merck)

Praseodymium (III) acetate hydrate ($\text{Pr}(\text{CH}_3\text{CO}_2)_3 \cdot \text{H}_2\text{O}$)(Alfa Aesar),

Hexamethylenetetramine (HMT) (Sigma Aldrich),

Methanol (CH_3OH), (Merck)

Monoethylamine ($\text{C}_2\text{H}_5\text{NH}_2$), (Merck).

3.2 Characterization

3.2.1 X-ray Diffraction (XRD)

X-ray powder diffraction patterns were recorded by using Rigaku Multiflex 2kW diffractometer. Copper is the most common target material with Cu $K\alpha$ λ : 1.5418 Å radiation. Scan range were presented as peak positions at 2θ and the angles between 20° - 80° . Scan speed arrange as $5^\circ/\text{min}$ (cullity 1978).



Figure 3.8. Rigaku MultiFlex 2kW Diffractometer

3.2.2 Scanning electron microscope (SEM) and energy dispersive study(EDS)

SEM-EDX graphs were taken by Joel model 6390 LV. JSM has a high resolution of 3.0 nm. The JSM-6390 has many properties that increase its versatility: super conical lens, smart settings for common samples, mechanically eucentric

stage, etc (JEOL - JSM-6390 - Scanning Electron Microscopes (SEM) □: HV/LV Tungsten/LaB6 SEMs - Scanning Electron Microscope by Jeol USA Inc n.d.).



Figure 3.9 Jeol model-JSM 6390 LV-;Scanning Electron Microscope

3.2.3 Chamber Furnaces

All the reactions have been carried out in an air with the aid of Protherm furnace PLF series (150/5). Respectively on the picture, one is tri-phase furnace: from 1400°C to 1600° C other one is mono-phase furnace: from 1100°C to 1600° C. In our experiment the samples were heated at 450-500° C.

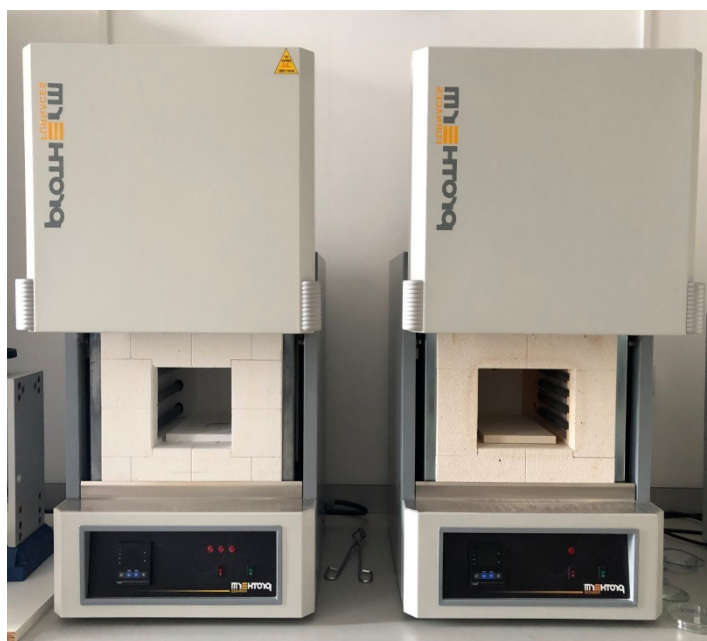


Figure 3.10 The PROTHERM FURNACE Chamber Furnace-PLF Series (150/5)

3.2.4 UV-VIS Diffuse Reflectance Spectra (UV-VIS-DRS)

UV-VIS spectrometers measure both diffuse and spectral reflectance. This can be arranged with the S/R change function. Diffuse reflectance is measured by settling the measurement sample next to the reflectance cell. Firstly, baseline was taken using the barium sulfate standard white plate. Then the standard white plate was taken and placed the measurement sample, started the measurement (Law n.d.). Also, Shimadzu UV-VIS can measure diffuse transmittance of solid, liquid and powders. The wavelength range is 220-1000 nm for this experiment was used 220-800 nm.



Figure 3.11 Shimadzu UV-VIS 2450 diffuse reflectance

3.2.5 RF Magnetron Sputtering

RF sputtering is an energetic wave through an inert gas in a vacuum chamber which becomes ionized. While sputtering were used forward P. 100 w, set pressure 50 mTorr.



Figure 3.12 Plasmalab 80 Plus RF sputter

3.3 Experimental Procedure

3.4 Preparation of ZnO films on PET and glass

ZnO films were placed on a disc rotating in a horizontal direction with respect to the target in both glass (~ 1.1 mm) and PET substrates (polyethylene terephthalate) using a RF sputtering technique and kept at ambient temperature. Er was doped on these substrates by hydrothermal method. Then, Erbium deposition on these ZnO coated substrates was performed using hydrothermal method.



Figure 3.13 Teflon-lined autoclave

3.4.1.1 Preparation of Er-doped ZnO films on glass substrate using hydrothermal method

ZnO coated glass substrates doped with Erbium. Zinc acetate dihydrate ($\text{Zn}(\text{CH}_3\text{COO})_2 \cdot 2\text{H}_2\text{O}$), erbium acetate tetrahydrate ($\text{Er}(\text{CH}_3\text{COO})_2 \cdot 4\text{H}_2\text{O}$), hexamethylenetetramine (HMT) these chemicals that are used in the experiment. Firstly, 0.2 M aqueous solution of Zinc acetate and Erbium acetate respectively 1%, 3%, 5%, 7%, 9% were dissolved in 20 ml distilled water. Then 0.56076 g HMT was added to each of the solution. Those solutions were stirred at magnetic stirring for 2 hours. ZnO doped glass substrates were horizontally put in the Teflon-lined autoclave. The solutions were added into the autoclaves. The reaction was occurred in an electric oven at 120° for 12 hours. Glass substrates were heated at 450° for 1 hour on chamber furnace before the fitting into autoclaves. After the hydrothermal process, glass substrates were out of autoclaves and dried in room temperature.

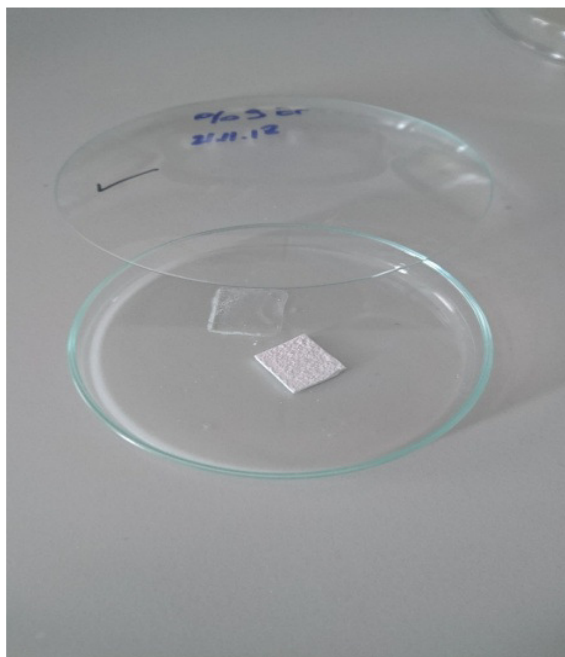


Figure 3.14 Er-doped glass substrate

3.4.1.2 Preparation of Er-doped ZnO films on PET substrate using hydrothermal method

In the experiment, ErAc ($\text{Er}(\text{CH}_3\text{COO})_2\cdot 4\text{H}_2\text{O}$), ZnAc ($\text{Zn}(\text{CH}_3\text{COO})_2\cdot 2\text{H}_2\text{O}$), hexamethylenetetramine were used as the chemicals. 0.2 M solution as 1%, 3%, 5%, 7%, 9% ErAc and ZnAc were dissolved in 20 ml distilled water. Then 0.56076 g HMT was added to every each of solution. Solutions were stirred at magnetic stirrer for 2 hours. PET substrates were settled in the Teflon-lined autoclaves which the coated part was stayed on the upper side. After that, they were put in the electric oven at 120° for 12 hours.

3.4.1.3 Preparation of Pr-doped ZnO films on glass substrate using hydrothermal method

In the Pr-doped part were used zinc acetate dihydrate, praseodymium (III) acetate hydrate in addition to methanol and monoethyleneamine as 2:1 ratio. 0.5 M 20 mL solutions were subsequently prepared as 1%, 2%, 3%, 4% and 5% percentages. They were stirred for 2 hours on magnetic stirrer. Glass substrates were heated at 450° for 1 hour on chamber furnace before the fitting into autoclaves. Then

glass substrates put in Teflon-lined autoclaves and solutions transferred into autoclaves. These reactions also were performed in an electric oven at 90° but the reaction time took almost 5 days. Pr-doped glass substrates were heated at 450° for 2 hours in chamber furnace. Then substrates were dried at room temperature. All the samples were labeled for characterization processes.

3.4.2 Preparation of Zn_{1-x}Er_xO nanoparticles by hydrothermal method (X=0.01, 0.03, 0.05, 0.07, 0.09)

In this part of experiment, ZnAc, ErAc, HMT were used as the chemicals 0.2 M aqueous solution of ZnAc, ErAc were dissolved in 20 ml distilled water. Every solution was added 0.56076 g HMT and stirred on magnetic stirrer for 2 hours. The solutions were poured in the Teflon-lined autoclaves. The reaction was occurred at 120° for 12 hours. After that Er-doped ZnO powder were filtered from solution by filtering and washed with deionized water. Those powders were heated at 450° for 2 hours on chamber furnaces. Then they were crushed using mortar and pestle until obtained a homogeneous solid mixture.

3.4.3 Preparation of Zn_{1-x}Pr_xO nanoparticles by hydrothermal method (X=0.01,0.02,0.03,0.04,0.05)

These chemicals used in the experiment are PrAc, ZnAc, HMT. By the same way 0.2 M equimolar solution of ZnAc, PrAc were prepared and dissolved in 20 ml distilled water. Then 0.56076 g HMT were added in every solution and stirred on magnetic stirrer for 2 hours. The solutions were put into autoclaves. Pr-doped ZnO powder was obtained from the solution by filtering. They were washed with deionized water and dried in room temperature. After that, all powders were heated at 500° for 30 minutes and dried in air. They were crushed for obtaining homogeneous powder. Pr-doped ZnO samples were labeled for the instrumentation.

4. RESULT AND DISCUSSION

4.1 ZnO films on glass substrates

4.1.1 X-ray Diffraction (XRD) study

Figure 16 shows the XRD pattern of pure ZnO on the glass. As can be seen from the figure that the ZnO film formed on the glass consists of the peaks of ZnO characteristic peaks. 2θ values of ZnO (ICDD:36-1451) 31.71 for 30° and 59.07 for 60° .

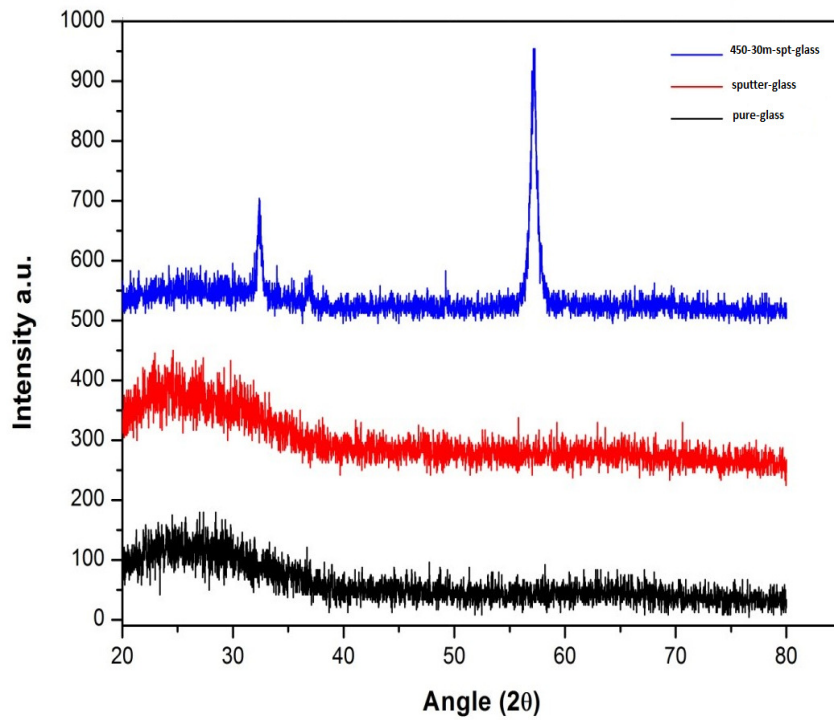


Figure 4.15 XRD patterns of ZnO film on glass substrate

4.2 Zn_{1-x}Er_xO films (x=0.03,0.05,0.07,0.09) on glass substrates

4.2.1 XRD study

In Fig4.17 was seen the XRD patterns of the Zn_{1-x}Er_xO films (x= 0.03, 0.05, 0.07, 0.09) on glass substrate. Also the Rietveld analysis was showed in Fig.17 to utilize the sample quality. The XRD patterns reveal that all the samples synthesized at 3%, 5%, 7%, 9% concentrations have wurtzite hexagonal structure with the preferred orientation along the (101) direction. No characteristic peaks related to Er and impurity peaks appear in XRD patterns in comparison with the Standard XRD patterns of ZnO (ICDD: 36-1451) which show that all Er atoms may entered into ZnO lattice. The hexagonal lattice constants a and c were calculated from the interplanar spacing, d_{hkl} , of (hkl) planes obtainable from XRD peaks and using the following equation.

$$\frac{1}{d_{hkl}^2} = \left[\frac{4}{3} \left(\frac{h^2 + hk + l^2}{a^2} \right) + \frac{l^2}{c^2} \right] \quad (4.2)$$

The lattice parameters a and c for Er-doped ZnO films are given in table 1. The average grain size (D) of samples were calculated using Scherrer's formula(de Sanctis et al. 1994) (Conference 1972).

$$D = \frac{0.9 \lambda}{B \cos \theta} \quad (4.3)$$

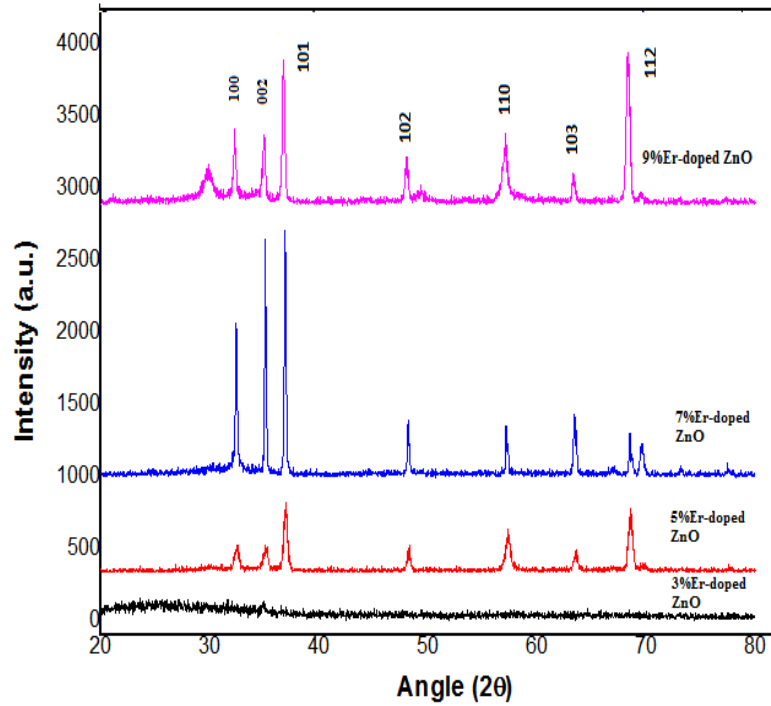
Where λ is the wavelength of incident X-ray $B = \sqrt{b_m^2 - b_0^2}$ line broadening, b_m and, b_0 are full width at half maximum of the XRD peak of the sample and the silicon standard. The average grain sizes were obtained using the full width half at half maximum of (101), (002), and (101) characteristic peaks and the results are listed in the table 1.

$$V = \frac{\sqrt{3}a^2c}{2} = 0.866a^2c \quad (4.4)$$

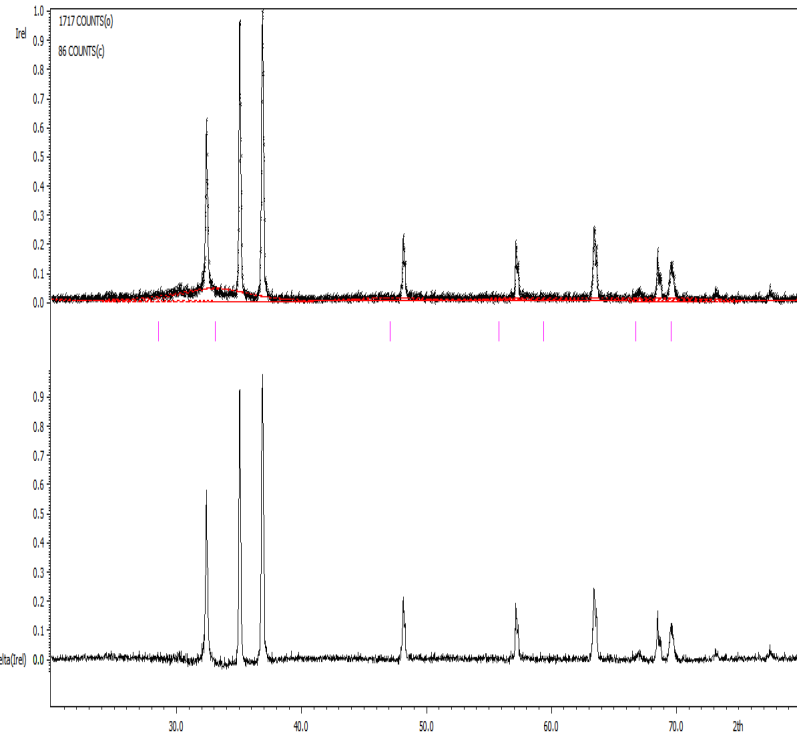
This formula gives the volume of the cell, a and c cell parameters. Following equation crystal lattice distortion degree and bond length formula,

$$R = \frac{2a\sqrt{2+3}}{c} \quad (4.5)$$

$$L = \sqrt{\frac{a^2}{3} + c^2\left(\frac{1}{2} - u^2\right)} \quad (4.6)$$



a)



b)
Figure 4.16 a) XRD patterns of $Zn_{1-x}Er_xO$ ($x= 0.03, 0.05, 0.07, 0.09$) on glass substrate **b)** $Zn_{0.93}Er_{0.07}O$ XRD profile fitting from Rietveld analysis

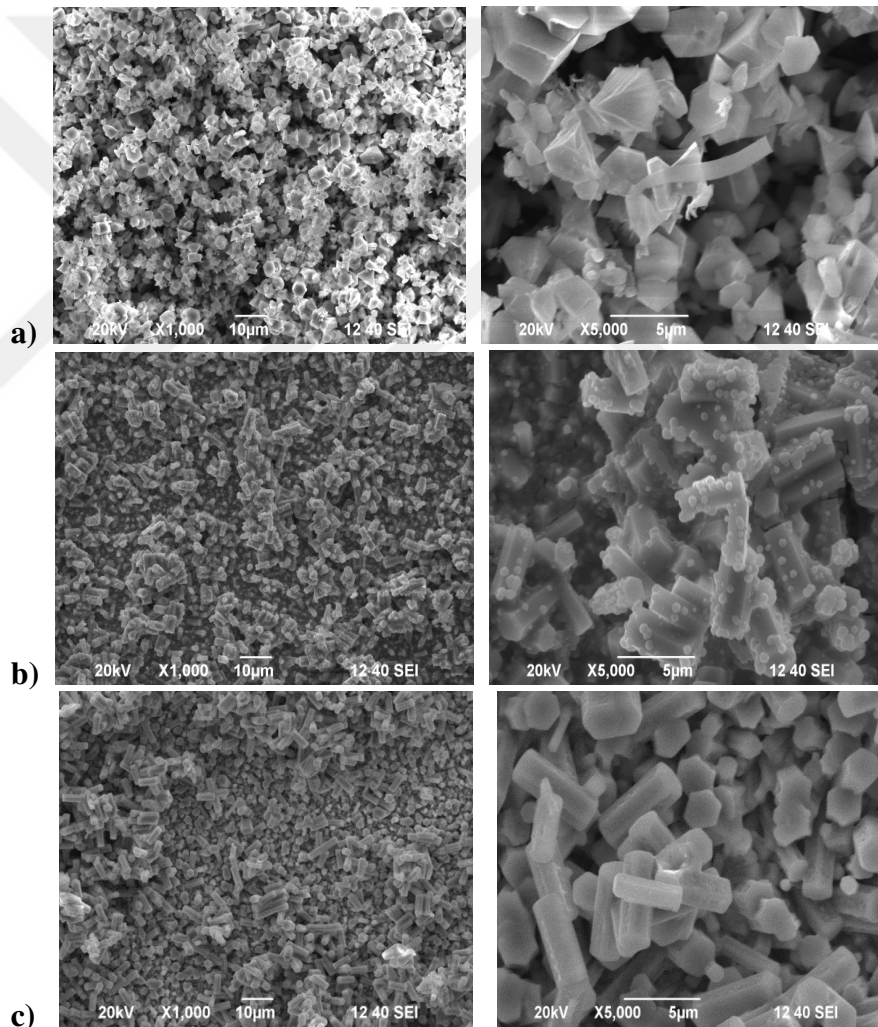
After the Rietveld analysis were obtained the data values. The a and b cell parameters are the same c is different because of the hexagonal structure. XRD patterns matched with the ZnO pattern that the space group P63mc. The goodness of fit (GOF), expected profile (R_p) and weighed profile (R_{wp}) were calculated. These values are 4.86, 56.22 and 67.36 respectively (Behdadfar et al. 2010). Also, the calculated cell parameters are $a=b= 3.1169$ and $c= 4.8634$ (S. D. Senol,2019).

Table 4.1. Concentration-dependent average particle sizes, lattice parameters, atomic packing factor (c/a), crystal lattice distortion degree and volume of the unit cell $Zn_{1-x}Er_xO$ thin films on glass substrate

Sample Name	a(Å)	c(Å)	c/a	Grain size from XRD(nm)	R	L(ZnO)	V
$Zn_{0.97}Er_{0.03}O$	3.203	5.138	1.604	142.88	1.017	1.980	45.64
$Zn_{0.95}Er_{0.05}O$	3.180	5.106	1.605	15.15	1.017	1.964	44.71
$Zn_{0.93}Er_{0.07}O$	3.189	5.116	1.604	69.73	1.017	1.971	45.05
$Zn_{0.91}Er_{0.09}O$	3.171	5.092	1.605	54.27	1.016	1.959	44.33

4.2.2 Scanning electron microscopy SEM and energy dispersive X-ray EDX study

The SEM figures of the $Zn_{1-x}Er_xO$ films ($x = 0.03, 0.05, 0.07, 0.09$) on glass substrates are shown in Fig.18 respectively. These figures clearly show that the formation of hexagonal ZnO nanostructures varied with different Er dopant ions. The shape of images are seem that spheroid-pyramidal like structure of $Zn_{0.97}Er_{0.03}O$ and rod-like structures of $Zn_{0.95}Er_{0.05}O$, $Zn_{0.95}Er_{0.05}O$, and obelisk-shaped nanorods grown on glass substrate of $Zn_{0.91}Er_{0.09}O$ Fig.18 shows the EDX spectrum of a) $Zn_{0.97}Er_{0.03}O$ b) $Zn_{0.95}Er_{0.05}O$ c) $Zn_{0.93}Er_{0.07}O$ d) $Zn_{0.91}Er_{0.09}O$ respectively (Baruah and Dutta 2009), (Djurišić and Leung 2006).



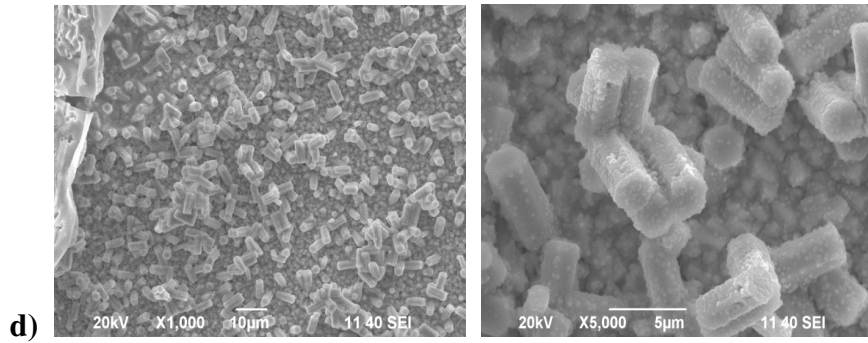
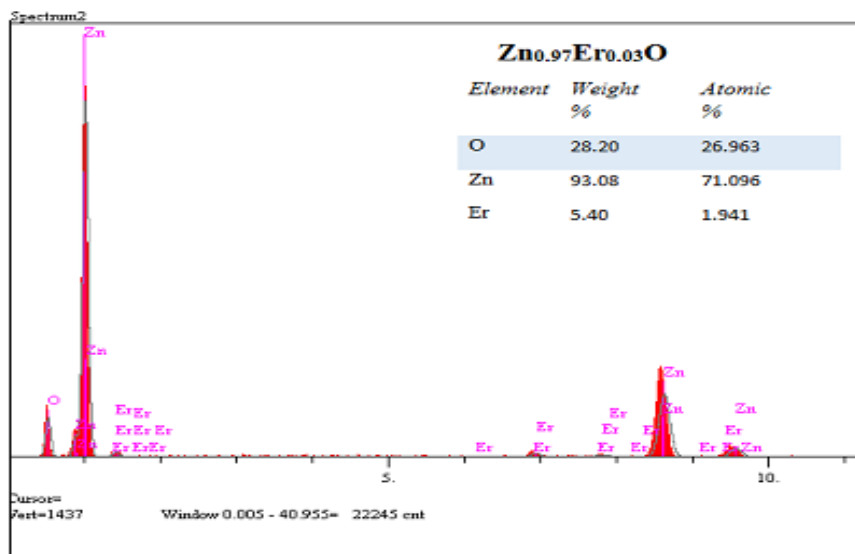
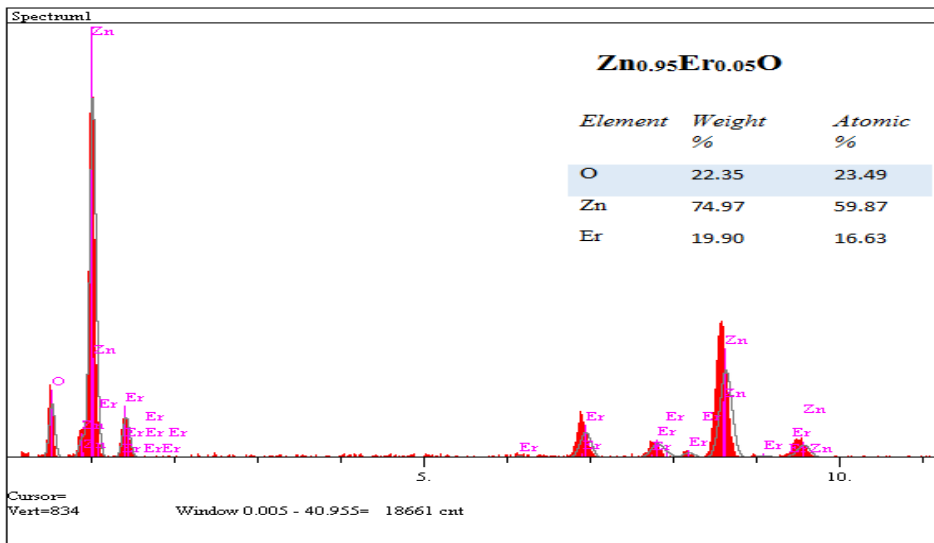


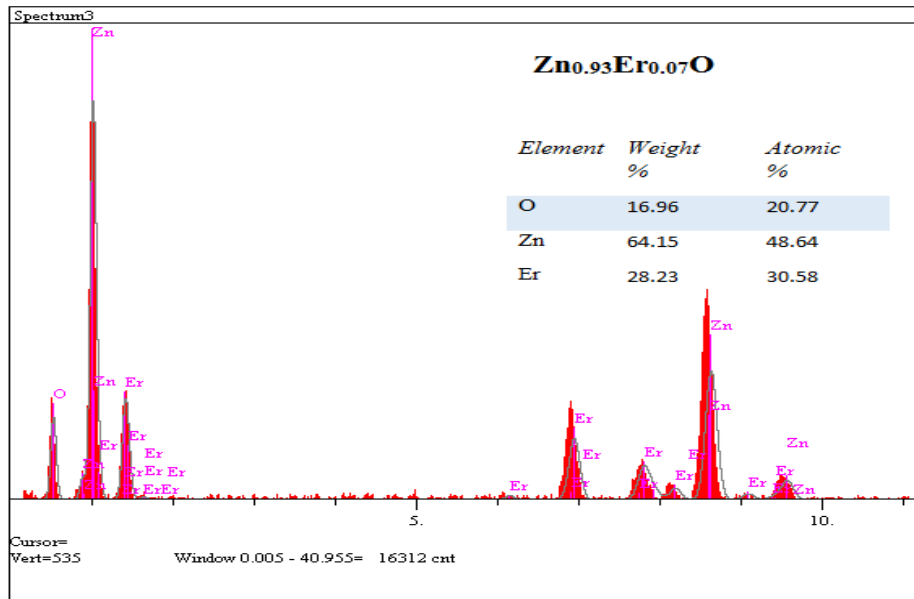
Figure 4.17 SEM images of the $Zn_{1-x}Er_xO$ ($x=0.03, 0.05, 0.07, 0.09$) on glass substrates respectively with 10 μm magnification 5 μm magnification



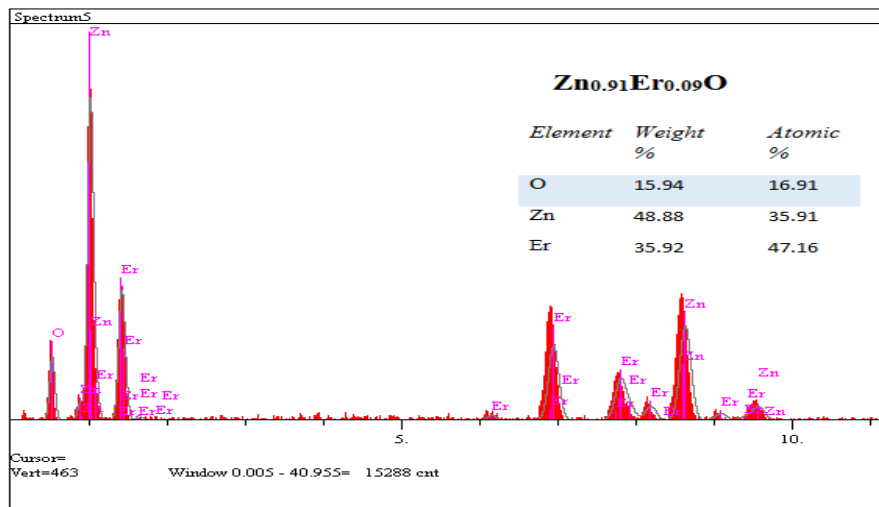
a)



b)



c)



d)

Figure 4.18 EDS image of the $Zn_{1-x}Er_xO$ films a) $Zn_{0.97}Er_{0.03}O$ b) $Zn_{0.95}Er_{0.05}O$ c) $Zn_{0.93}Er_{0.07}O$ d) $Zn_{0.91}Er_{0.09}O$ respectively

4.2.3 Optical properties

The optical transmission spectra in the range of 325 nm and 600 nm for samples on glass substrate at room temperature are shown in Fig.20. The optical band gaps of the prepared $Zn_{1-x}Er_xO$ films ($x= 0.01, 0.03, 0.05, 0.07, 0.09$) on glass substrate are calculated using the Tauc equation (Brian et al. 2015). Tauc method was used for simple wavelengths absorption spectroscopy, sensor coatings, films and other applications. Because of the using Tauc method, studied on simple stoichiometry material to form many chemical ways of ZnO. To evaluating the Tauc method the ZnO is very useful due to widely studied in many applications. The optical absorption strength depends on between the photon energy and the band gap energy as shown in equation 7.

$$(\alpha h\nu)^{1/n} = A(h\nu - E_g) \quad (4.7)$$

Where h is Planck's constant, ν is the photon's frequency, α is the absorption coefficient, E_g is the bandgap and A is constant. The value of the exponent meaning the electronic transition: for direct allowed transition $n=1/2$, direct forbidden transitions $n=3/2$, indirect allowed transitions $n=2$, indirect forbidden transitions $n=3$. The allowed transitions are dominate ones, and the other ones are respectively.

The optical band gap of the samples were determined by plotting the $(\alpha h\nu)^2$ versus photon energy ($h\nu$) and extra plotting the linear portion of the respective curve to the $h\nu$ axis gave the optical band gap value (E_g). The dependence of $(\alpha h\nu)^2$ on $h\nu$ is shown in figure 21. From this figure, obtained E_g values $Zn_{0.99}Er_{0.01}O$, $Zn_{0.97}Er_{0.03}O$, $Zn_{0.95}Er_{0.05}O$, to $Zn_{0.93}Er_{0.07}O$ which are 2.99 eV, 3.02 eV, 3.15 eV, and 3.18 eV respectively. While the bandgap energy values increased to 1,3,5,7 % Er concentration, it decreased for the 9% sample. The band gap energy value for the $Zn_{0.91}Er_{0.09}O$ samples is calculated as 3.05 eV.

The obtained E_g values of films are observed to shift towards the lower wavelength (higher energy) region (blue shift) meaning there is a blue shift with increasing Er content (1%, 3%, 5%, and 7%). The reason of this, reduces of ZnO nanorods may lead to a higher energy. (Sevim D. Senol et al. 2019).

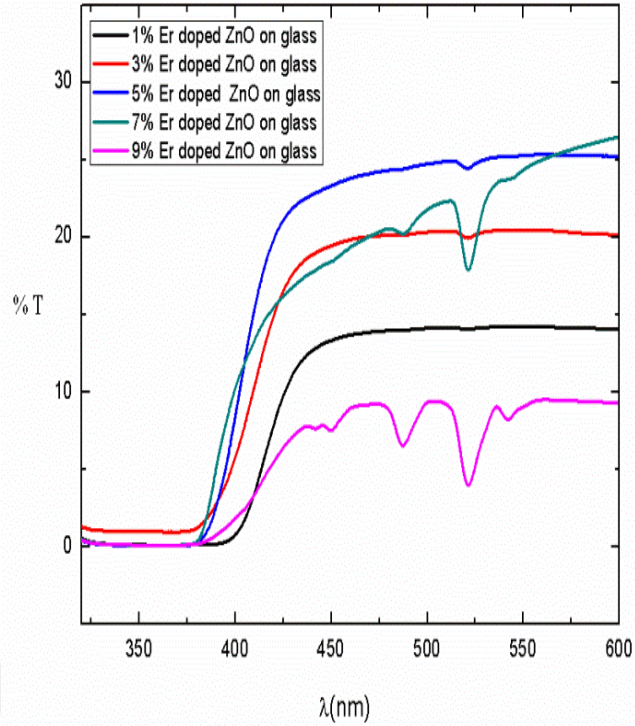


Figure 4.19 Optical transmittance spectra of $Zn_{1-x}Er_xO$ films ($x= 0.01, 0.03, 0.05, 0.07, 0.09$) on glass substrate

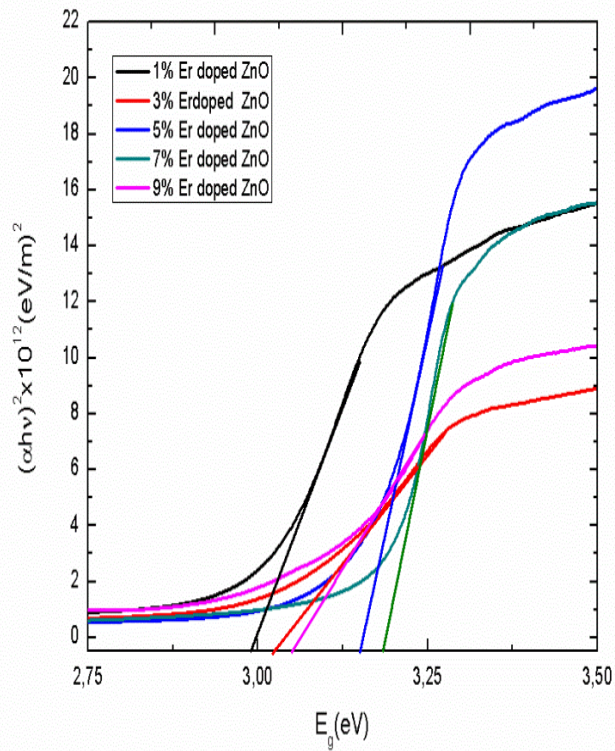
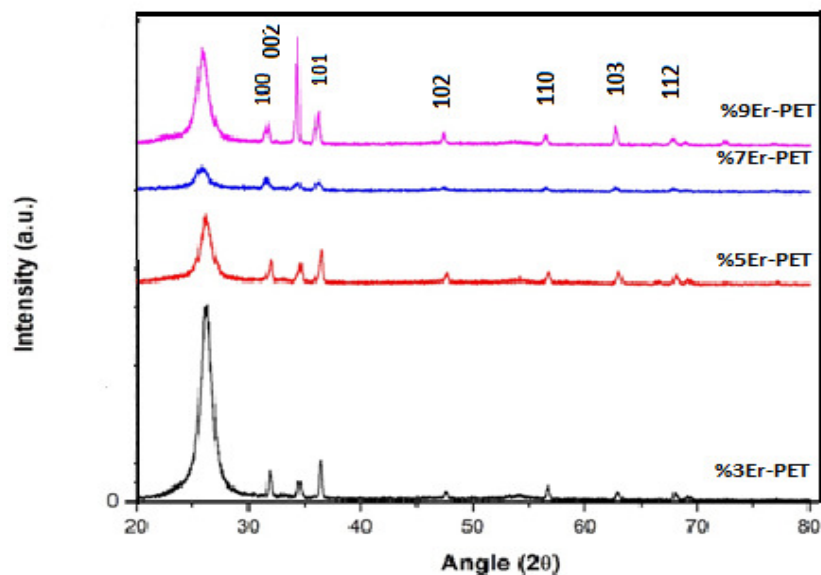


Figure 4.20 The plots of $(\alpha h\nu)^2$ versus photon energy ($h\nu$) of $Zn_{1-x}Er_xO$ films ($x=0.01, 0.03, 0.05, 0.07, 0.09$) on glass substrate

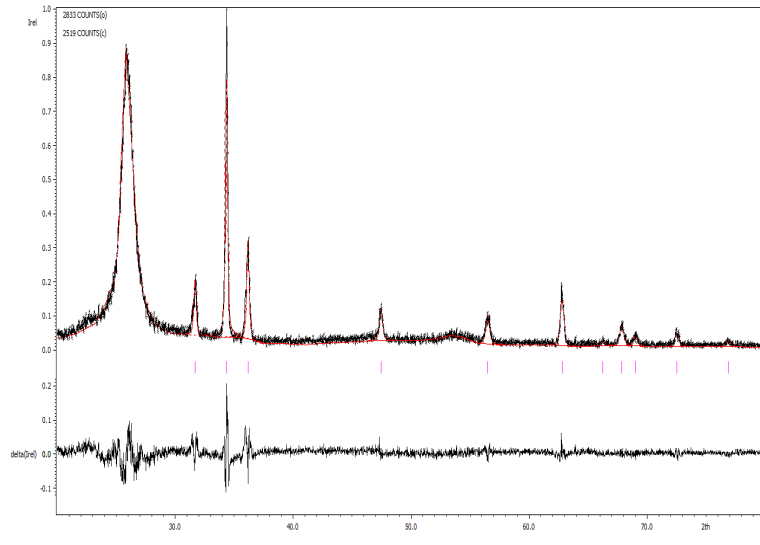
4.3 Zn_{1-x}Er_xO films (x=0.03, 0.05, 0.07, 0.09) on PET substrate

4.3.1 XRD studies

The XRD patterns of Zn_{1-x}Er_xO films (x=0.03, 0.05, 0.07, 0.09) on PET substrate are shown in Fig.22. Except the diffraction peaks at 26° which are due to the PET substrates, the reason of decreases of these picks related to increases of Pr concentrations. The films exhibit the ZnO (100), (002) and (101) diffraction peaks, and the first three peaks is the major peak, indicating that the films are hexagonal wurtzite structure with a preferential orientation along the c-axis perpendicular to the substrates. And no diffraction peak of Er₂O₃ is observed, which reveals all Er atoms entering the ZnO crystal lattice. Using XRD analysis of Zn_{1-x}Er_xO films (x=0.03, 0.05, 0.07, 0.09) on PET substrate samples the concentration-dependent average nanorod sizes (D), lattice parameters, volume of the unit cell (V), and bond length (L) were determined, and reported in table 2. Additionally, the Rietveld analysis was performed for Zn_{0.91}Er_{0.09}O in Fig.22 to purify the sample quality.



a)



b)

Figure 4.21 a) XRD patterns of $Zn_{1-x}Er_xO$ ($x=0.03, 0.05, 0.07, 0.09$) on PET substrate b) the XRD profile fitting from the Rietveld analysis of $Zn_{0.91}Er_{0.09}O$

The goodness of fit (GOF): 2.90, expected profile (R_p): 16.57, and weighed profile (R_{wp}): 21.97 were calculated from the Rietveld analysis for $Zn_{0.91}Er_{0.09}O$. Also the cell parameters $a=b= 3.2506 \text{ \AA}$ and $c= 5.2044 \text{ \AA}$.

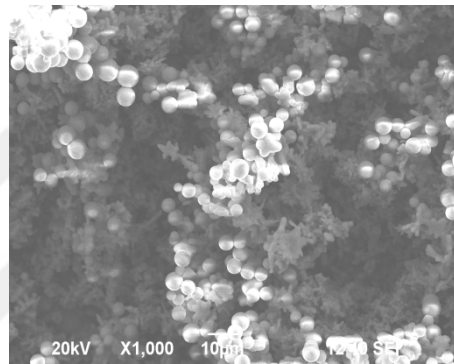
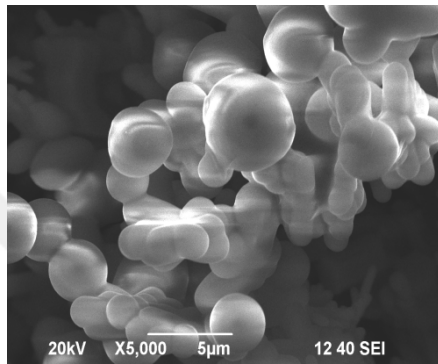
As for $Zn_{0.91}Er_{0.09}O$ nanorods grown on glass substrate the lattice parameter c calculated from the (002) peaks of the samples is 5.214 \AA and that for the $Zn_{0.97}Er_{0.03}O$ is 5.188 \AA . The increase of the lattice parameter (about 0.026 \AA) indicate that Er is put into the ZnO crystal lattice and substituted for the Zn^{+2} sites (Li, Liu, and Zheng 2014). These changes are in fact to be expected if Er ions replace Zn ions in the lattice, hence the Er ions bigger ionic radii (0.89 \AA) than Zn ions (0.74 \AA).

Table 4.2. Cell parameters, crystallite sizes, bond lengths, crystal lattice distortion degree and volume of unit cell of $Zn_{1-x}Er_xO$ thin films on PET substrate

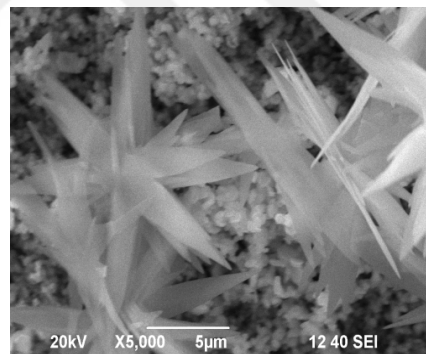
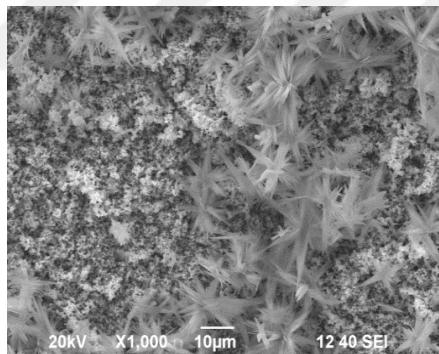
Sample Name	a (Å)	c (Å)	c/a(Å)	Grain size			
				from XRD(nm)	L (ZnO)	R	V
$Zn_{0.97}Er_{0.03}O$	3.235	5.188	1.603	24.78	2.000	1.018	47.01
$Zn_{0.95}Er_{0.05}O$	3.226	5.172	1.603	33.66	1.996	1.018	46.61
$Zn_{0.93}Er_{0.07}O$	3.265	5.206	1.594	83.63	2.026	1.024	48.05
$Zn_{0.91}Er_{0.09}O$	3.255	5.214	1.601	240.12	2.014	1.019	47.83

4.3.2 SEM-EDS Studies

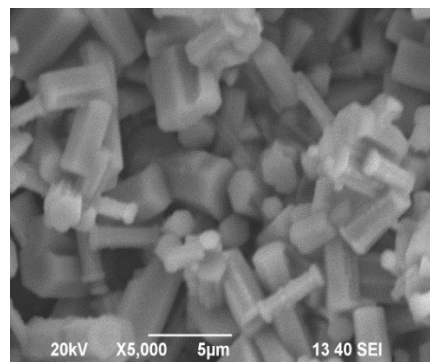
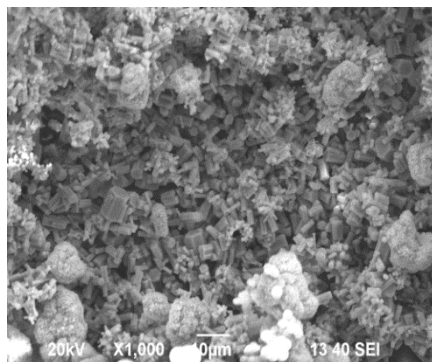
The SEM figures of the $Zn_{1-x}Er_xO$ films ($x=0.03, 0.05, 0.07, 0.09$) on PET substrates are shown in Fig.23 respectively. These SEM figures show that the formation of hexagonal nanostructures. The $Zn_{0.97}Er_{0.03}O$ has cluster of grapes like ZnO structure, the $Zn_{0.95}Er_{0.05}O$ flower-like shaped, and the $Zn_{0.93}Er_{0.07}O$, $Zn_{0.91}Er_{0.09}O$ have nanorods shaped. The composition of $Zn_{1-x}Er_xO$ thin films were investigated by EDX measurements. Zn, Er, and O peaks are clearly seen and the content of Zn, O and, Er are consisted with preparation of thin films.



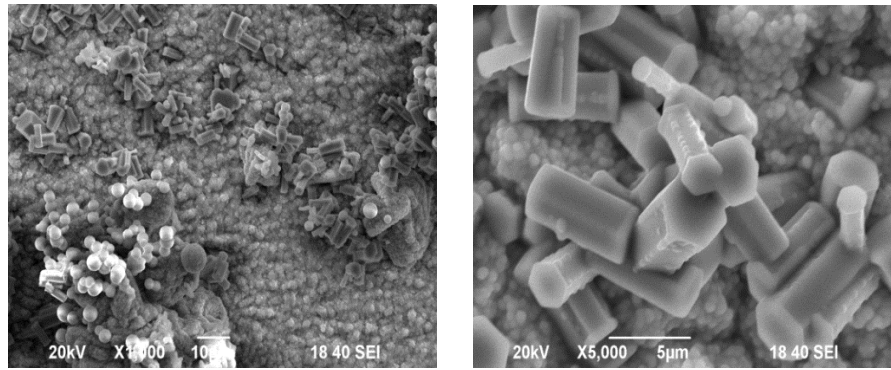
a) $Zn_{0.97}Er_{0.03}O$



b) $Zn_{0.95}Er_{0.05}O$

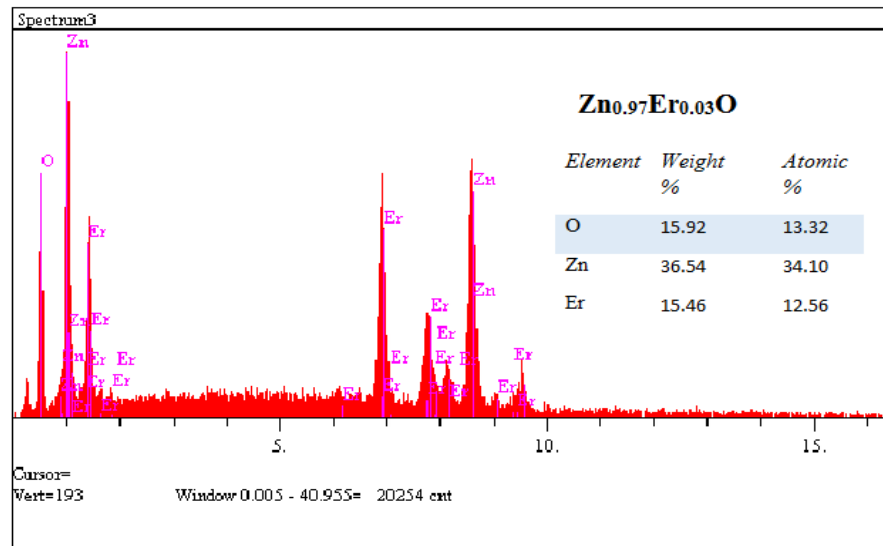


c) $Zn_{0.93}Er_{0.07}O$

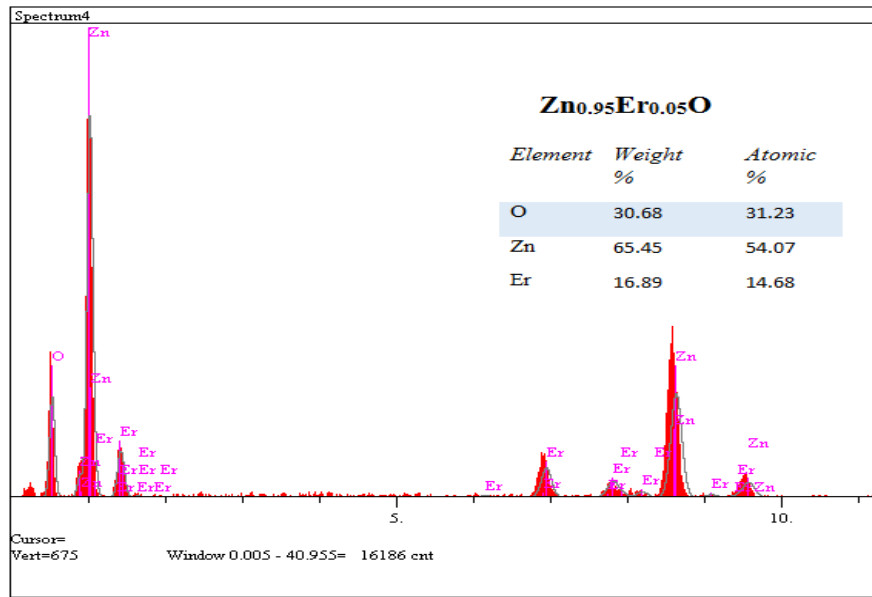


d) $Zn_{0.91}Er_{0.09}O$

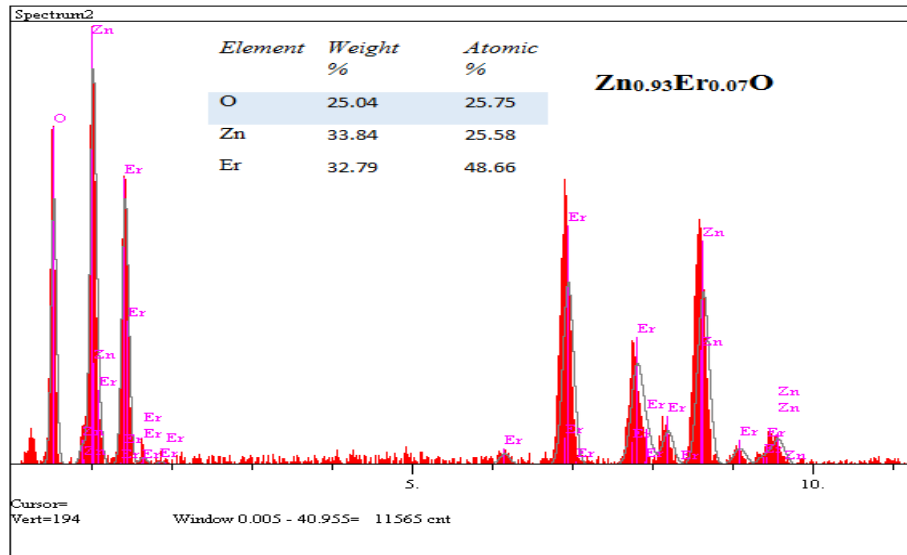
Figure 4.22 SEM images of the $Zn_{1-x}Er_xO$ ($x= 0.03, 0.05, 0.07, 0.09$) on PET substrates respectively with 10 μm magnification and 5 μm magnification



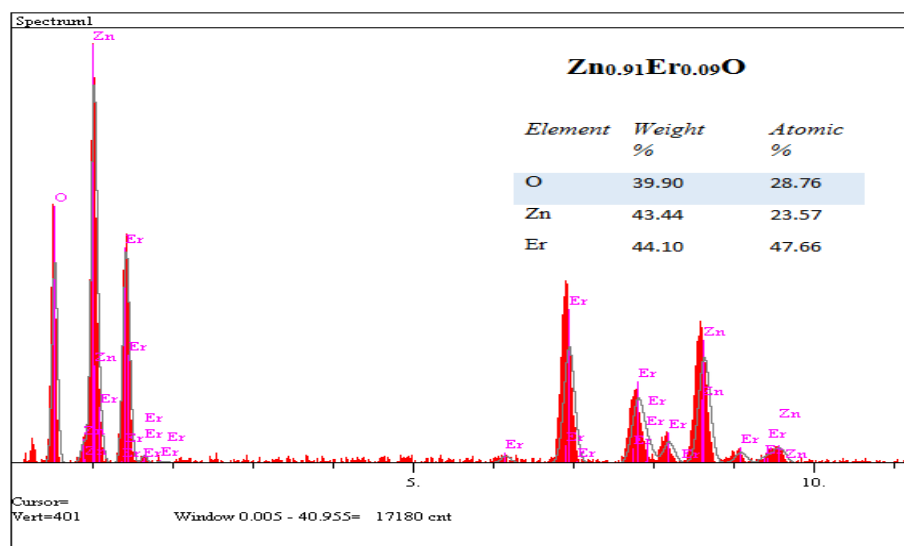
a)



b)



c)



d)

Figure 4.23 EDX image of the $Zn_{1-x}Er_xO$ films ($x=0.03, 0.05, 0.07, 0.09$) on PET substrate a) $Zn_{0.97}Er_{0.03}O$ b) $Zn_{0.95}Er_{0.05}O$ c) $Zn_{0.93}Er_{0.07}O$ d) $Zn_{0.91}Er_{0.09}O$ respectively

4.3.3 Optical Properties

The optical transmission spectra of $Zn_{1-x}Er_xO$ films ($x=0.03, 0.05, 0.07, 0.09$) on PET substrates were recorded over the wavelength range 220–800 nm at room temperature (Fig.25). The band gap energy (E_g), as shown in figure 26, were found by the slope of the graph of the $(\alpha hv)^2$ versus photon energy (hv) and extrapolating the linear spare of the respective curve to the hv axis gave the optical band gap value (E_g).

The obtained band gap energy values are 3.19 eV for undoped ZnO, 3.14 eV for $Zn_{0.97}Er_{0.03}O$, 3.15 eV for $Zn_{0.95}Er_{0.05}O$, 3.16 eV, and 3.17 eV respectively. The broadening of optical band gap with increase in Er doping concentration is verified as expected. The optical absorption edge of Er-doped ZnO nanofilms shifted towards higher energy values blue shift. The shift in the optical absorption edge with Er doping concentration may be related to the partial filling of conduction band by the free caries due to the blocking of lower states and by virtue of compositional variation which is known as Burstein-Moss effect.

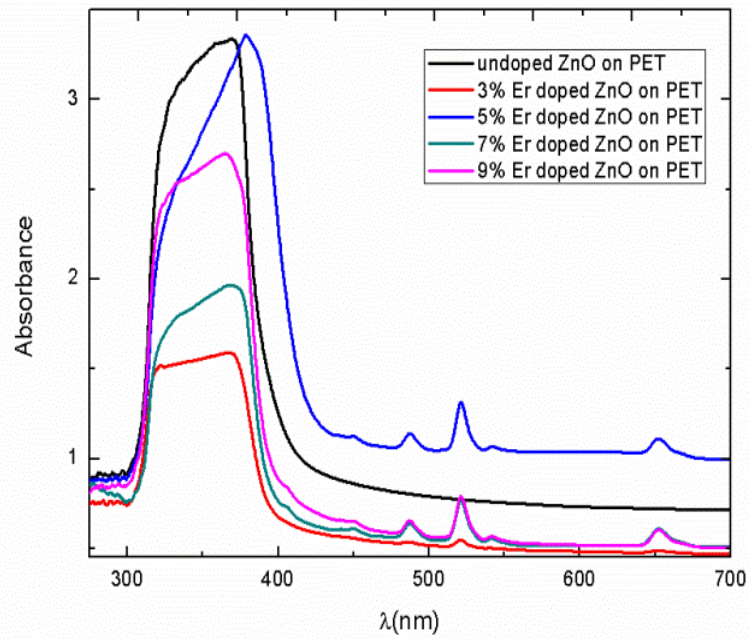


Figure 4.24 Optical absorbance spectra of $Zn_{1-x}Er_xO$ films ($x= 0.03, 0.05, 0.07, 0.09$) on PET substrate

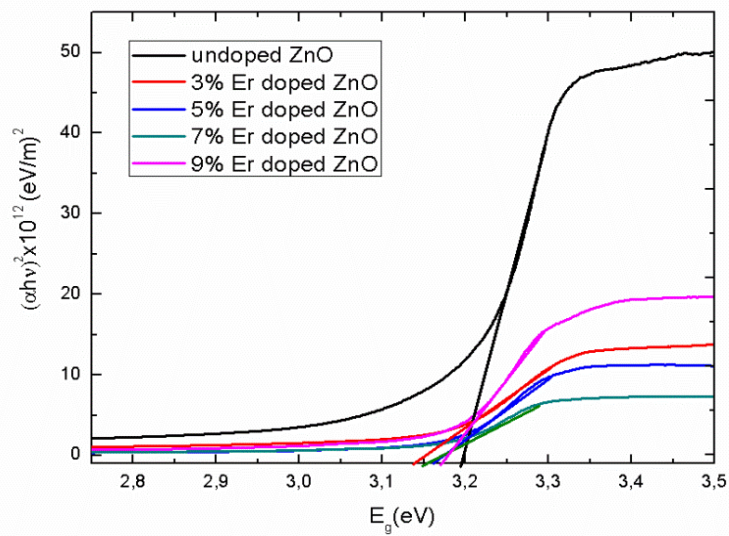
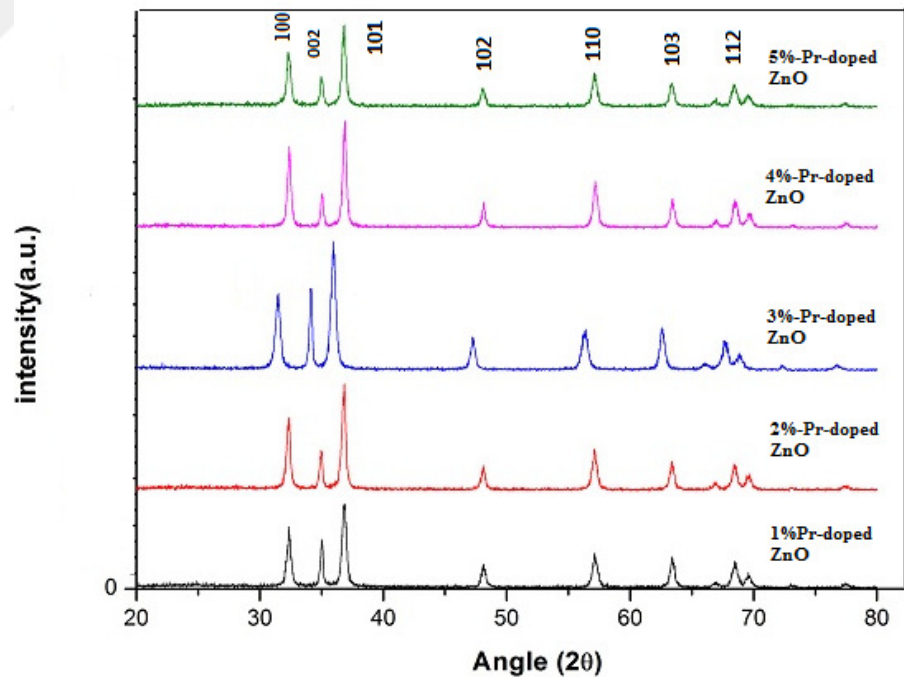


Figure 4.25 The plots of $(\alpha h\nu)^2$ versus photon energy ($h\nu$) of $Zn_{1-x}Er_xO$ films ($x= 0.03, 0.05, 0.07, 0.09$) on PET substrate

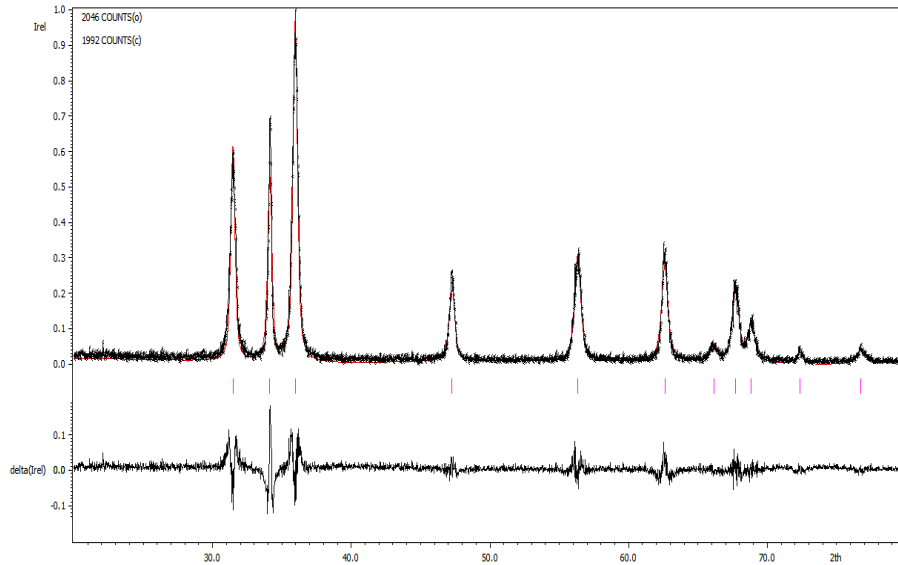
4.4 Zn_{1-x}Pr_xO films (x=0.01, 0.02, 0.03, 0.04, 0.05) on glass substrate

4.4.1 XRD Study

Figure.27 shows the XRD patterns of the Zn_{1-x}Pr_xO films (x=0.01, 0.02, 0.03, 0.04, 0.05) on glass substrate. The XRD patterns reveal that all the sample synthesized at 1%, 2%, 3%, 4%, 5% concentrations have hexagonal wurtzite structure (ICDD: 36-1451). The hexagonal lattice constants a and c were calculated from the interplanar spacing, d_{hkl} of (hkl) planes obtainable from XRD peaks and using the formula 1 as was mentioned above. The Rietveld analysis was shown in Fig.25 for Zn_{0.97}Pr_{0.03}O. The goodness of fit: 3.28, expected profile: 14.54, and weighed profile: 21.05 were calculated from the Rietveld analysis for Zn_{0.97}Pr_{0.03}O. The cell parameters a=b= 3.2900 Å and c= 5.2400 Å.



a)



b)

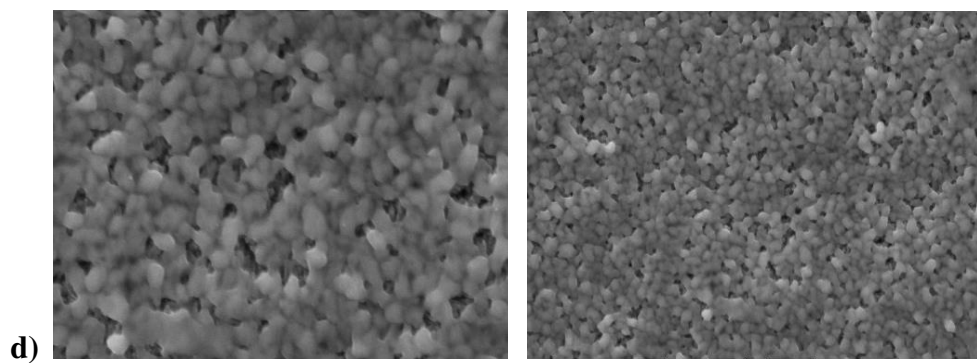
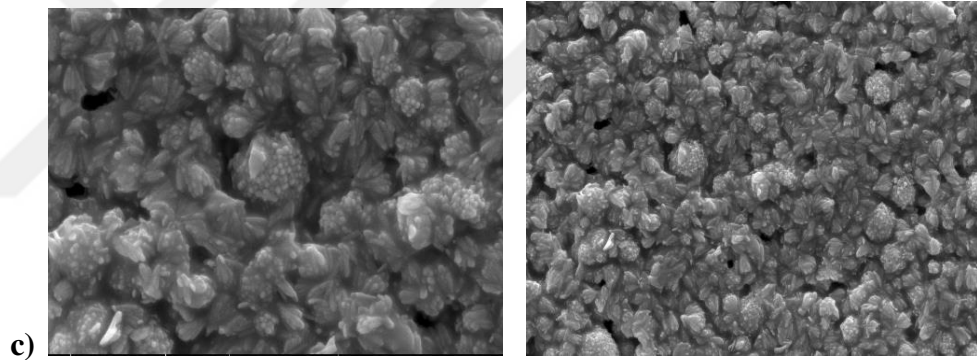
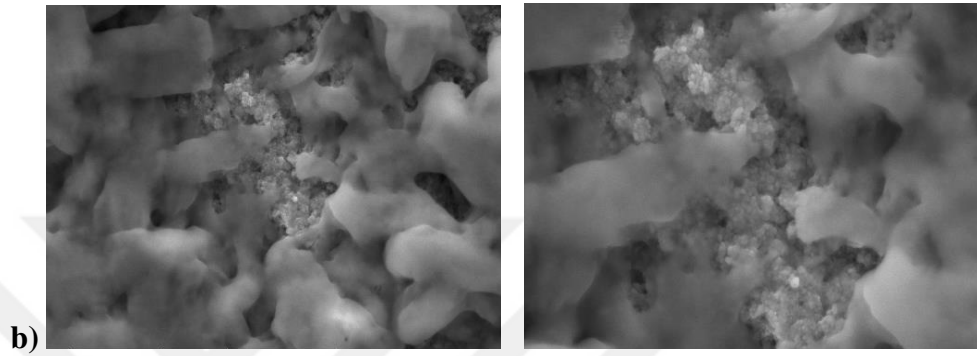
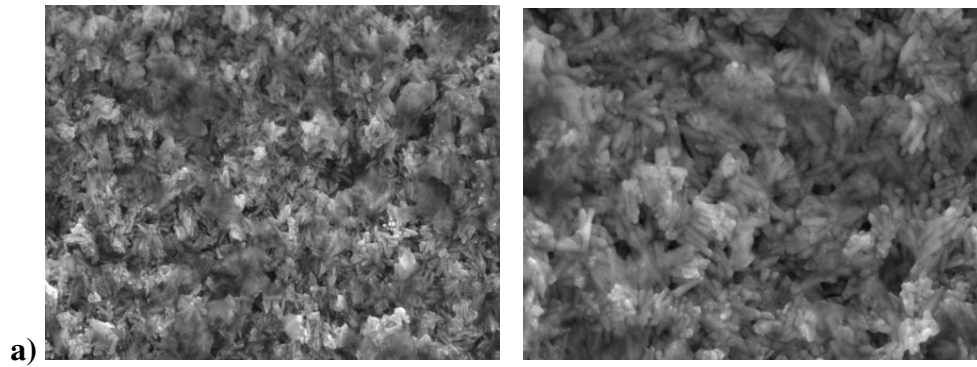
Figure 4.26 a) XRD patterns of $Zn_{1-x}Pr_xO$ ($x=0.01, 0.02, 0.03, 0.04, 0.04$) on glass substrate **b)** the XRD profile fitting from Rietveld analysis of $Zn_{0.97}Pr_{0.03}O$

Table 4.3. Cell parameter, atomic packing factor (c/a), particle sizes, bond length, crystal lattice distortion degree, and volume of unit cell $Zn_{1-x}Pr_xO$ thin films on glass substrate.

Sample Name	a (Å)	c(Å)	c/a(Å)	Grain size from XRD(nm)	L(ZnO)	R	V
$Zn_{0.99}Pr_{0.01}O$	3.191	5.120	1.604	20.13	1.973	1.017	45.14
$Zn_{0.98}Pr_{0.02}O$	3.193	5.128	1.606	21.47	1.972	1.016	45.27
$Zn_{0.97}Pr_{0.03}O$	3.279	5.248	1.600	21.13	2.030	1.020	48.86
$Zn_{0.96}Pr_{0.04}O$	3.188	5.118	1.605	24.21	1.971	1.017	45.04
$Zn_{0.95}Pr_{0.05}O$	3.193	5.126	1.605	20.19	1.974	1.017	45.25

4.4.2 SEM-EDS

The SEM figures of the $Zn_{1-x}Pr_xO$ films ($x=0.01, 0.02, 0.03, 0.04, 0.05$) on glass substrates are shown in the Fig.28, and EDX spectra in Fig.29 respectively. Pr doped ZnO images were taken 10 μm magnification and 5 μm magnification. The shapes of $Zn_{0.99}Pr_{0.01}O$, $Zn_{0.98}Pr_{0.02}O$, $Zn_{0.97}Pr_{0.03}O$, $Zn_{0.96}Pr_{0.04}O$, and $Zn_{0.95}Pr_{0.05}O$ were not taken clearly because of that the obtained substances were quite little. Figure 29 shows the EDX result find out the samples of Zn and O with a trace quantity of Pr element.



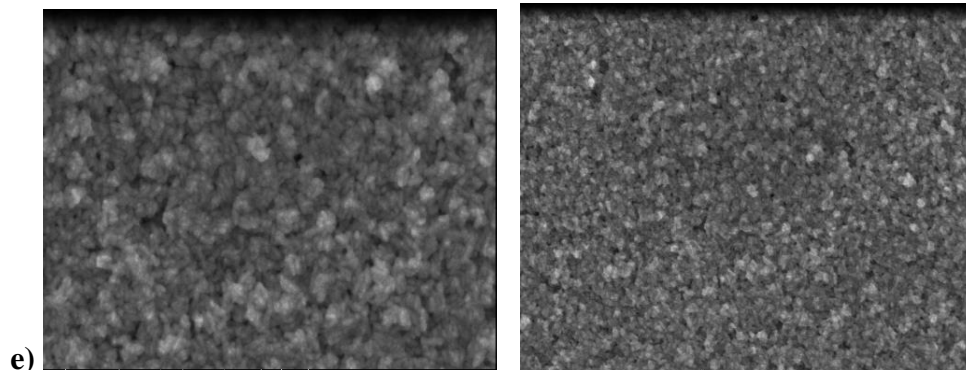
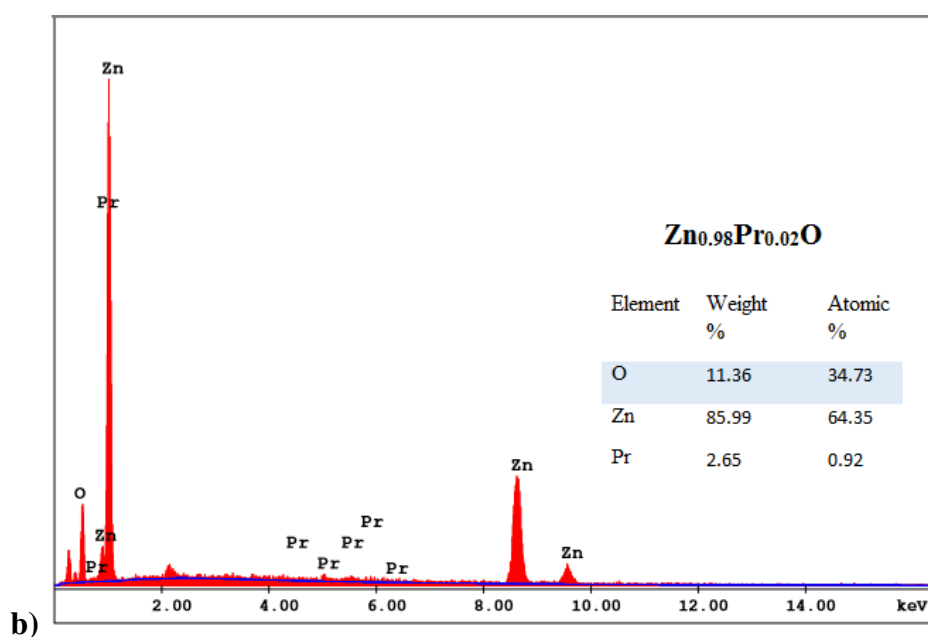
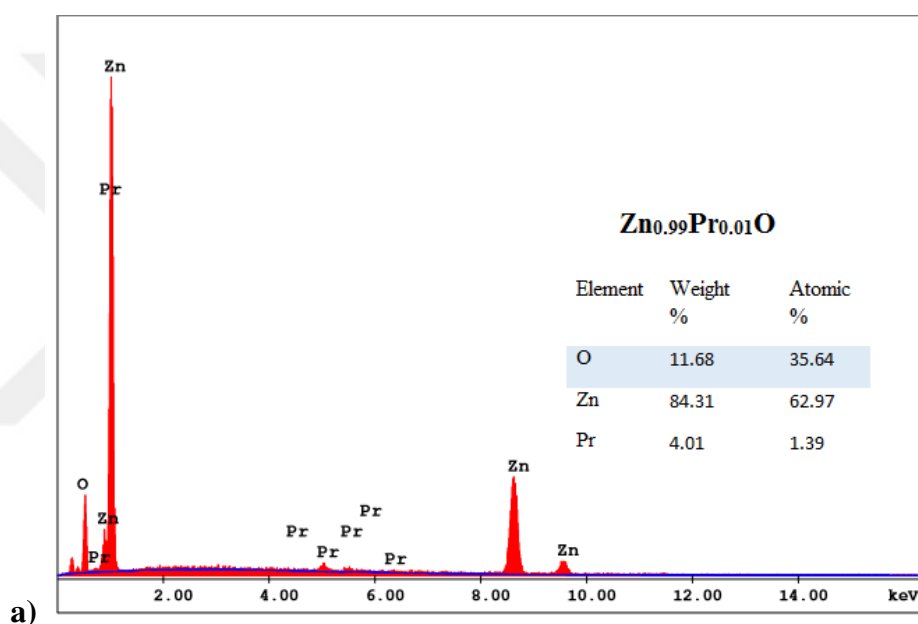
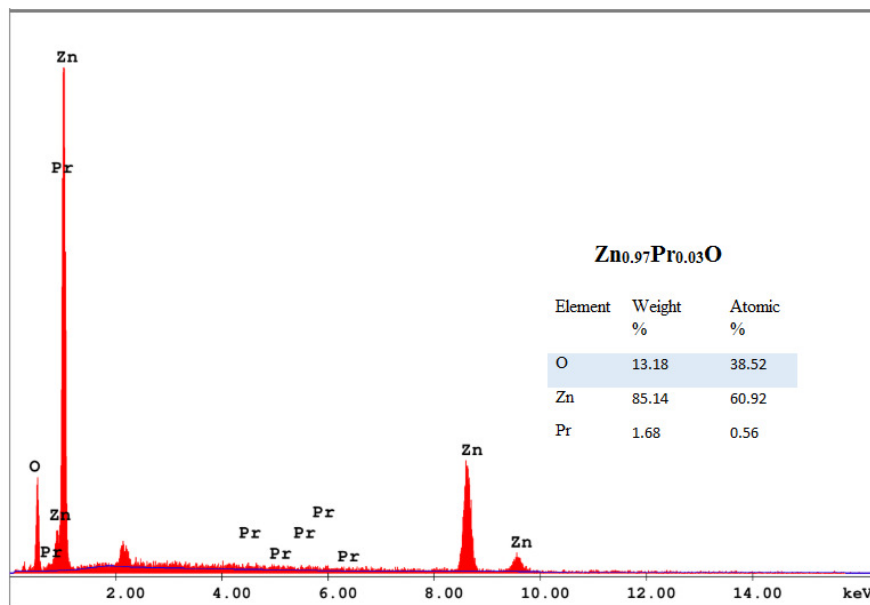
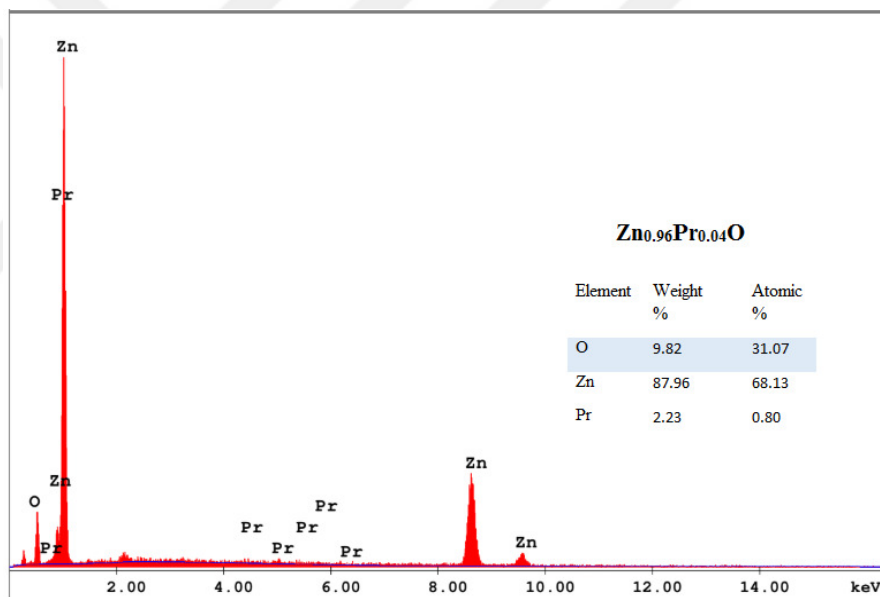


Figure 4.27 SEM images of 1%, 2%, 3%, 4%, 5% $Zn_{1-x}Pr_xO$ films a) $Zn_{0.99}Pr_{0.01}O$ b) $Zn_{0.98}Pr_{0.02}O$ c) $Zn_{0.97}Pr_{0.03}O$ d) $Zn_{0.96}Pr_{0.04}O$ e) $Zn_{0.95}Pr_{0.05}O$ respectively with 10 μm magnification and 5 μm magnification

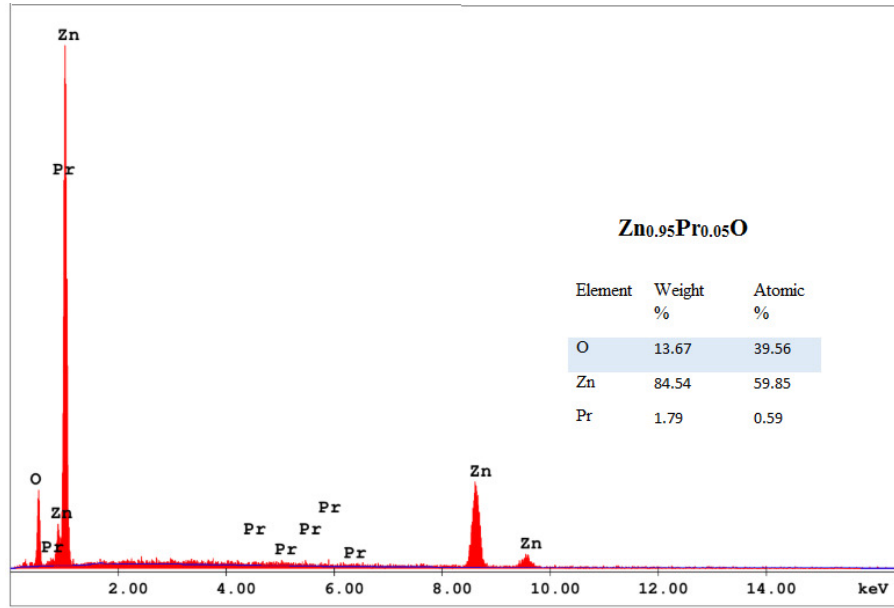




c)



d)



e)

Figure 4.28 EDX image of the Zn_{1-x}Pr_xO nanoparticles **a)** Zn_{0.99}Pr_{0.01}O **b)** Zn_{0.98}Pr_{0.02}O **c)** Zn_{0.97}Pr_{0.03}O **d)** Zn_{0.96}Pr_{0.04}O **e)** Zn_{0.95}Pr_{0.05}O respectively

4.4.3 Optical Properties

The UV-VIS optical absorption spectra of the Zn_{1-x}Pr_xO films (x= 0.01, 0.02, 0.03, 0.04, 0.05) on glass substrates are shown in Fig.30. The optical band gaps of the prepared Zn_{1-x}Pr_xO thin films are calculated using the Taug equation. The optical band gap of the samples were determined by plotting the $(\alpha h\nu)^2$ versus photon energy (hν) and extra plotting the linear portion of the respective curve to the hν axis gives the optical band gap value (E_g). The dependence of $(\alpha h\nu)^2$ on hν is shown in Fig.31. The variation of E_g values with Pr content for ZnO films which is shown in Figure 31. The obtained E_g values are 2.99 eV Zn_{0.99}Pr_{0.01}O, 2.64 eV Zn_{0.98}Pr_{0.02}O, 3.04 eV Zn_{0.97}Pr_{0.03}O, 3.07 eV Zn_{0.96}Pr_{0.04}O, 2.28 eV Zn_{0.95}Pr_{0.05}O respectively.

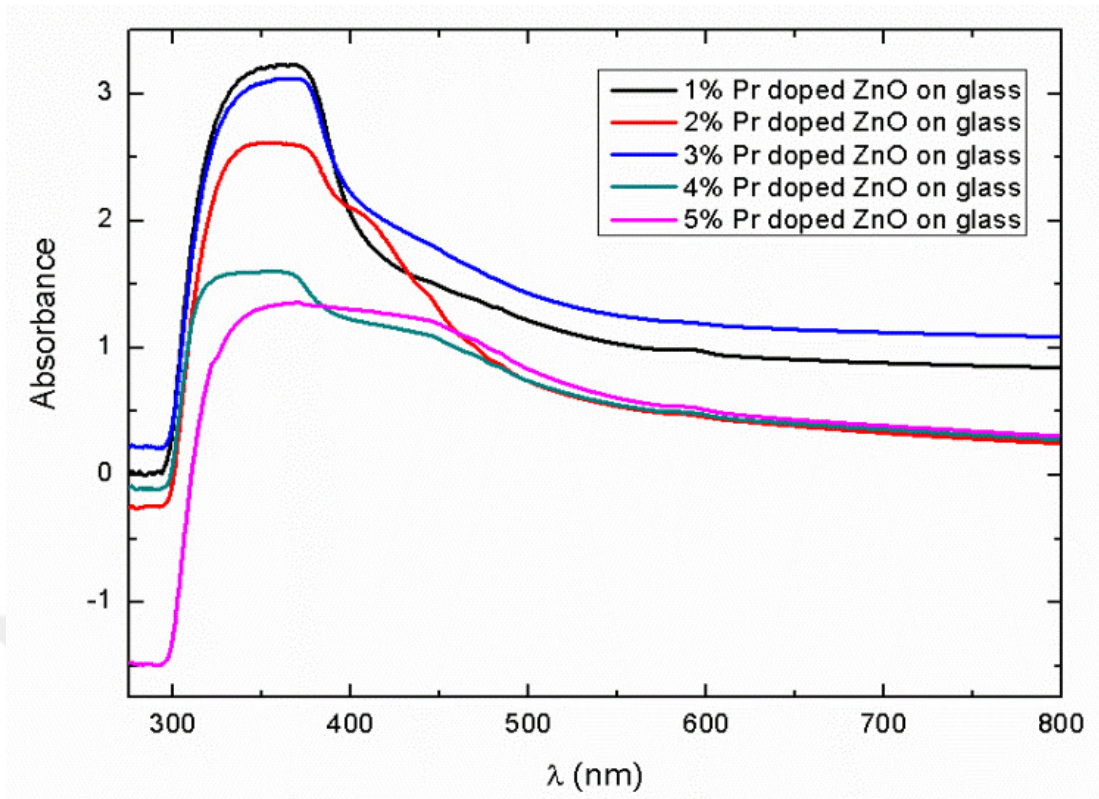


Figure 4.29 Absorbance spectra of $Zn_{1-x}Pr_xO$ films ($x = 0.01, 0.02, 0.03, 0.04, 0.05$) on glass substrate

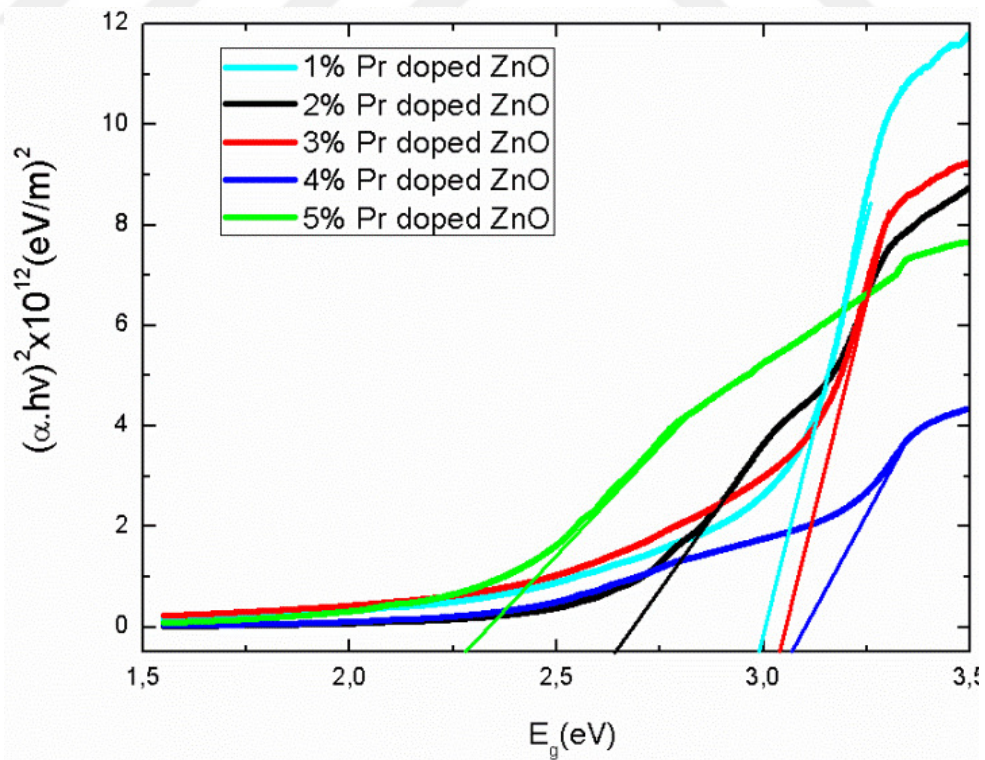


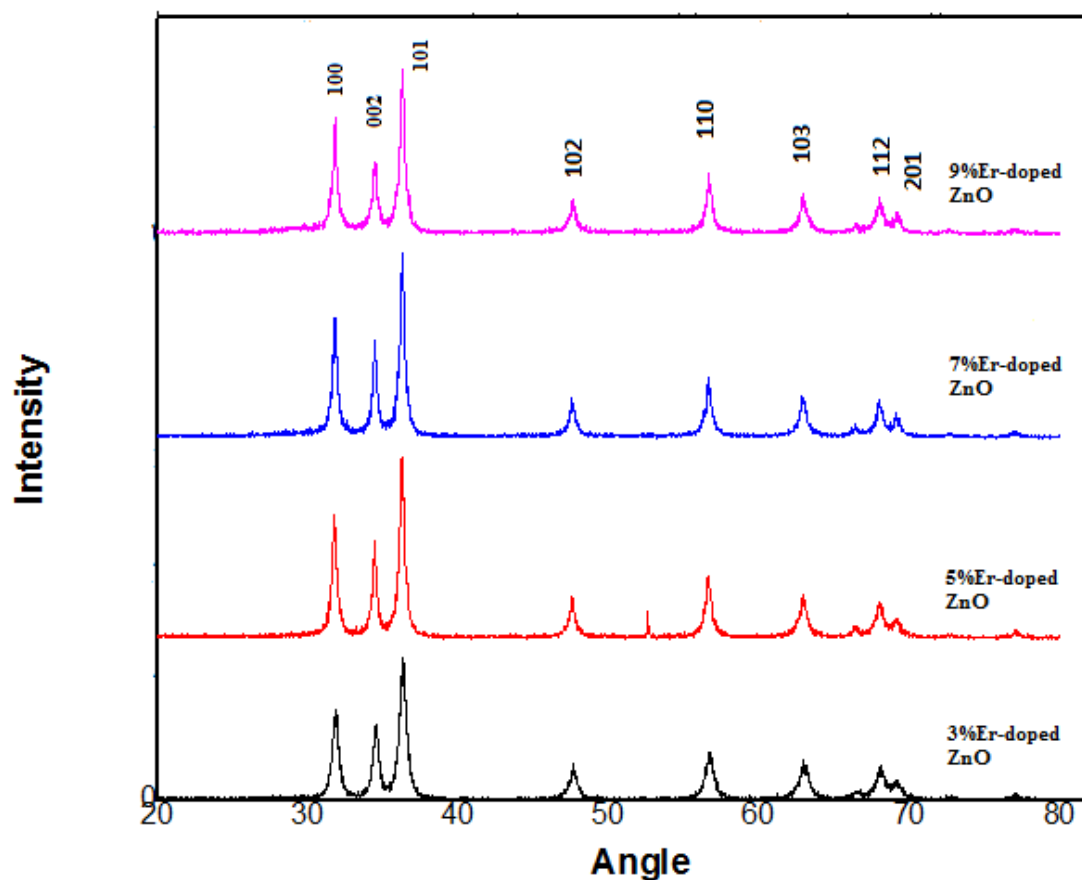
Figure 4.30 The plots of $(\alpha h\nu)^2$ versus photon energy ($h\nu$) of $Zn_{1-x}Pr_xO$ films ($x = 0.01, 0.02, 0.03, 0.04, 0.05$) on glass substrate

4.5 Preparation of $Zn_{1-x}Er_xO$ nanoparticles by hydrothermal method ($x= 0.03, 0.05, 0.07, 0.09$)

4.5.1 XRD Study

Figure 32 indicates the XRD patterns of $Zn_{1-x}Er_xO$ nanoparticles ($x=0.03, 0.05, 0.07, 0.09$). Main peaks that (100), (002), (101) shows the hexagonal wurtzite structure of substance. All Er atoms were entered in ZnO lattice. The extension was observed in the orientation of peak (101). And, a and c cell parameters were calculated that given by Table 4.4. The Rietveld analysis were shown in Fig.32.b for $Zn_{0.93}Er_{0.07}O$. The goodness of fit (GOF), expected profile (R_p) and weighed profile (R_{wp}) were calculated from the Rietveld analysis for $Zn_{0.91}Er_{0.09}O$. These values are 3.01, 21.09 and 27.59 respectively. The cell parameters $a=b= 3.2520 \text{ \AA}$ and $c= 5.2400 \text{ \AA}$.

a)



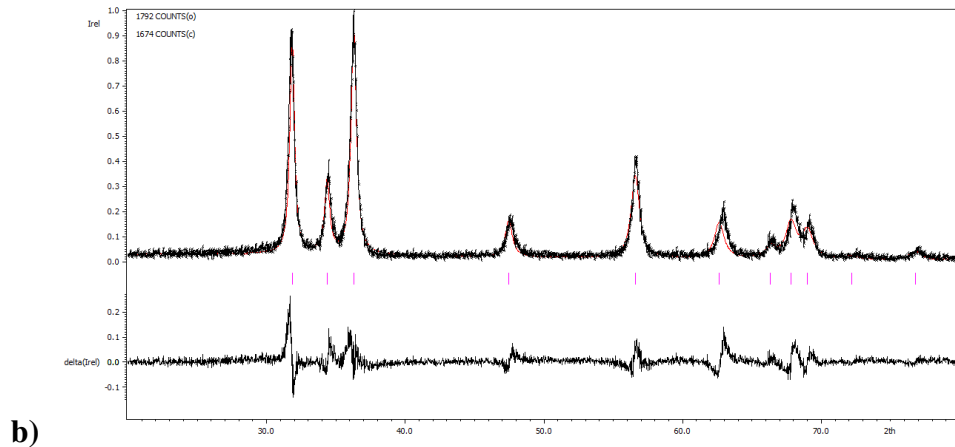


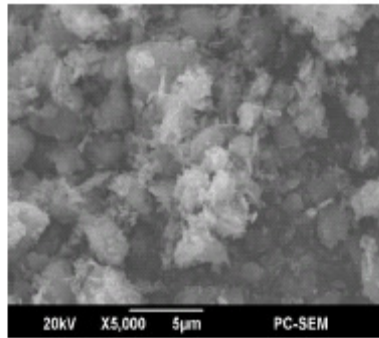
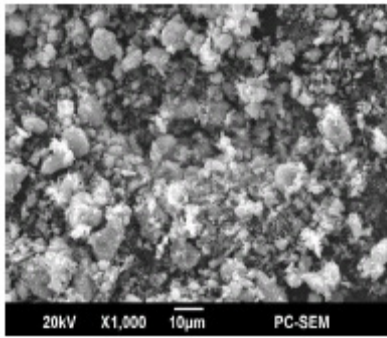
Figure 4.31 a) XRD patterns of $Zn_{1-x}Er_xO$ nanoparticles ($x = 0.03, 0.05, 0.07, 0.09$) b) the XRD profile fitting from Rietveld analysis of $Zn_{0.93}Er_{0.07}O$

Table 4.4. Cell parameters, atomic packing factor, average particle size, crystal lattice distortion degree, bond length and volume of the cell $Zn_{1-x}Er_xO$ nanoparticles.

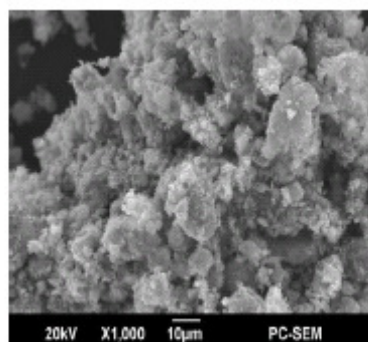
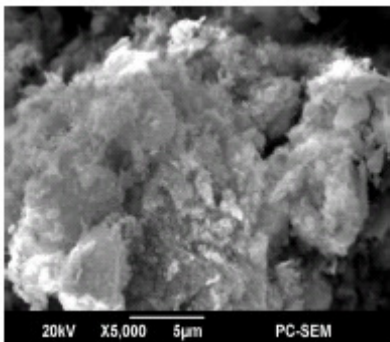
Sample Name	a(Å)	c(Å)	c/a	Grain size from XRD(nm)	R	L(ZnO)	V
$Zn_{0.97}Er_{0.03}O$	3.237	5.188	1.602	13.09	1.018	2.003	47.08
$Zn_{0.95}Er_{0.05}O$	3.248	5.204	1.602	19.51	1.019	2.009	47.54
$Zn_{0.93}Er_{0.07}O$	3.244	5.202	1.603	20.01	1.018	2.007	47.40
$Zn_{0.91}Er_{0.09}O$	3.242	5.199	1.603	20.59	1.018	2.004	47.31

4.5.2 SEM-EDS Study

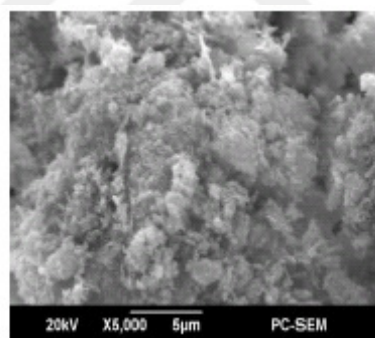
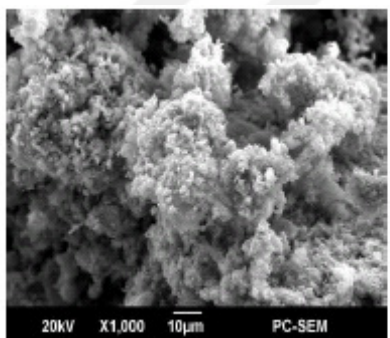
The SEM figures of the $Zn_{1-x}Er_xO$ ($x = 0.03, 0.05, 0.07, 0.09$) nanoparticles are seen in Fig.33. It is observed that the more or less spherical shape of prepared nanoparticles. Analysis of SEM images exposed almost uniform size distribution and grain boundaries with a bit agglomeration. The chemical composition of $Zn_{1-x}Er_xO$ nanoparticles were investigated EDX spectroscopy. Fig.34 shows the EDX spectra of $Zn_{1-x}Er_xO$ a) $x = 0.03$, b) $x = 0.05$, c) $x = 0.07$, d) $x = 0.09$ nanoparticles. Zn, O, and Er peaks are clearly seen and the content of Zn, O, Er are consistent with preparation of samples.



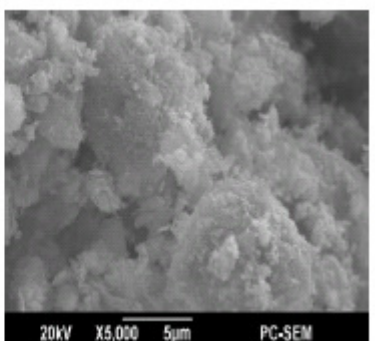
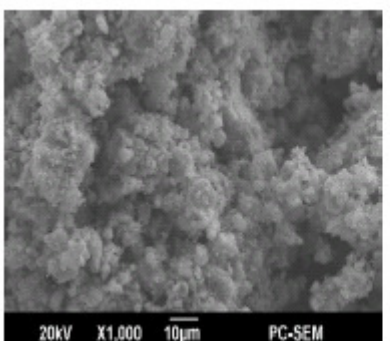
a) Zn_{0.97}Er_{0.03}O



b) Zn_{0.95}Er_{0.05}O

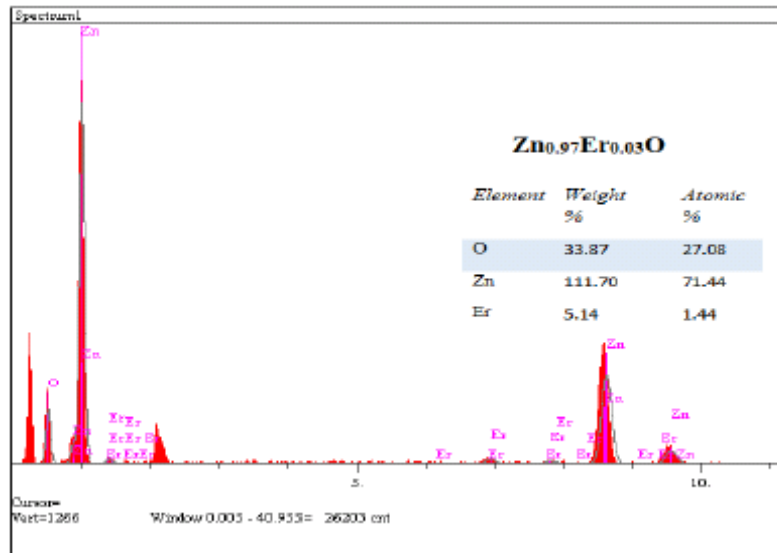


c) Zn_{0.93}Er_{0.07}O

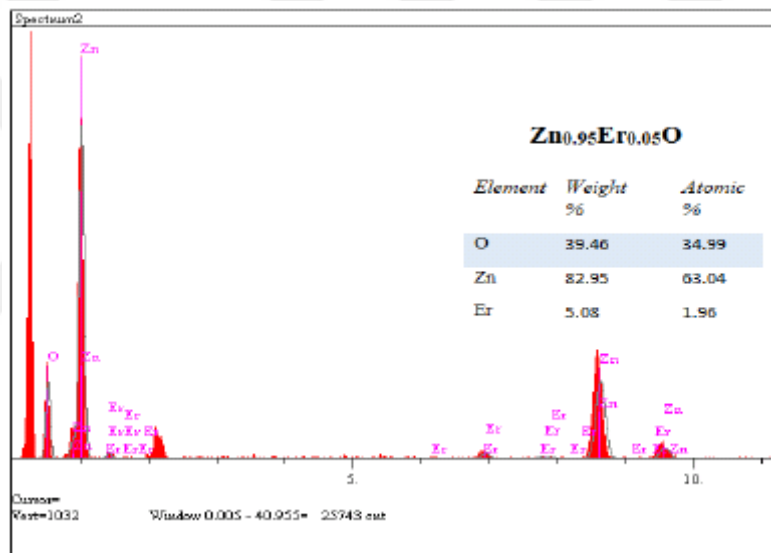


d) Zn_{0.91}Er_{0.09}O

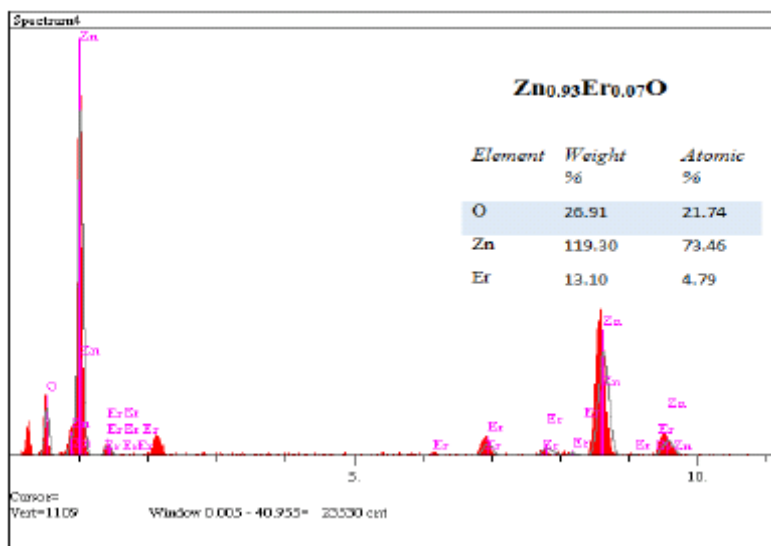
Figure 4.32 SEM images of the Zn_{1-x}Er_xO (x=0.03, 0.05, 0.07, 0.09) nanoparticles respectively with 10 μm and 5 μm magnification



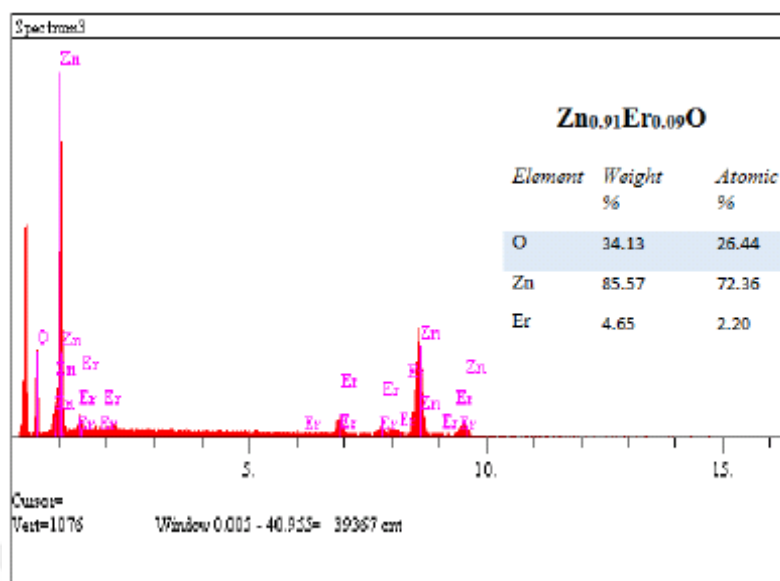
a)



b)



c)



d)

Figure 4.33 EDX images of Zn_{1-x}Er_xO nanoparticles a) Zn_{0.97}Er_{0.03}O b) Zn_{0.95}Er_{0.05}O c) Zn_{0.93}Er_{0.07}O d) Zn_{0.91}Er_{0.09}O respectively

4.5.3 Optical Properties

UV visible reflectance spectroscopy is a powerful technique to analyze optical properties of semiconductors. The reflectance depends on factor like the band gap, oxygen deficiency, surface roughness, and impurity centers. The diffuse reflection method is used to measure powder samples with a UV-VIS spectrophotometer. It involves using an integrating sphere to collect and measure the diffuse reflected light. In diffuse reflectance measurements, diffuse reflectance is proportional to concentration (Danckwerts, 2002).

The diffuse reflectance measurements carried out for all the Zn_{1-x}Er_xO nanoparticles (x= 0.03, 0.05, 0.07, 0.09) are presented in Fig.35. It was seen that the reflectance values changed with the increasing content of Er for whole spectral regions. The reflectance is above 90% for all samples wavelengths longer than 400 nm. A sharp decreases of reflectance intensity is observed at approximately around 375 nm for all samples. The reflectance edge of the samples have monotonous blue shift to lower wavelength (higher energy) up to 5% Er doping level. There is a shift of the reflectance edge to high wavelengths (red shift) for 7% Er. For 9% Er, shift of

the reflectance edge to low wavelength (blue shift) is observed. These shifts may be result of crystalline quality of the film, grain size, strain, etc. The diffuse reflectance data can be used for calculating the energy band gap of powder samples. The wavelength at which the peak of the derivative occurs is used in the formula:

$$E_g = \frac{hc}{\lambda_{max}} \quad (4.8)$$

Where h and c represent Planck's constant and speed of the light, respectively.

The band gap energies of the samples can be calculated maxima of the $dR/d\lambda$ as a function of wavelength as shown in Fig.36. The band gap energy value is 3.17 eV for $Zn_{0.99}Er_{0.01}O$, 3.18 eV for $Zn_{0.07}Er_{0.03}O$, 3.19 eV for $Zn_{0.95}Er_{0.05}O$, 3.18 eV for $Zn_{0.93}Er_{0.07}O$, 3.19 eV for $Zn_{0.91}Er_{0.09}O$ respectively. These results show that the energy gap widens for samples up to 5% Er doping but it narrows for 7% Er sample and for 9%, the band gap energy expanded again (Caglar, Caglar, and Ilican 2016)

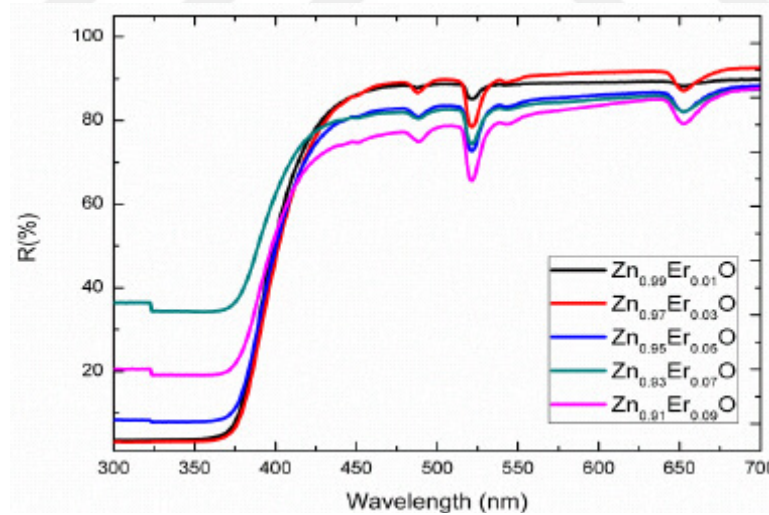


Figure 4.34 The reflectance spectra of the $Zn_{1-x}Er_xO$ ($x=0.01, 0.03, 0.05, 0.07, 0.09$) nanoparticles

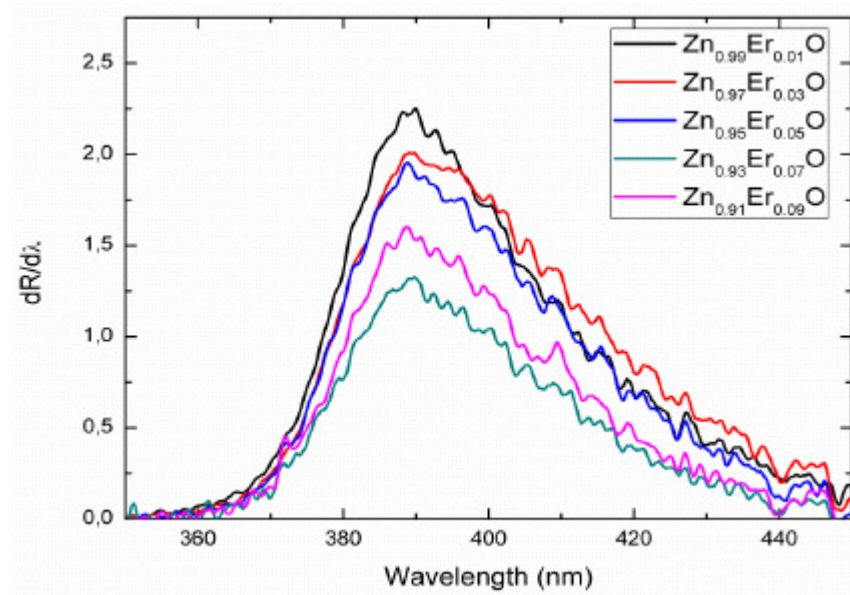
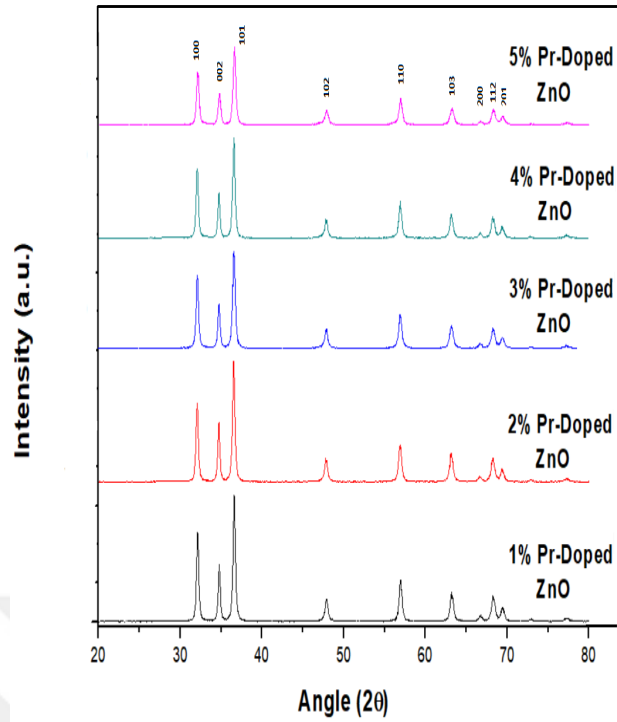


Figure 4.35 The plots of $dR/d\lambda$ as a function of wavelength for the $Zn_{1-x}Er_xO$ ($x=0.01, 0.03, 0.05, 0.07, 0.09$) nanoparticles

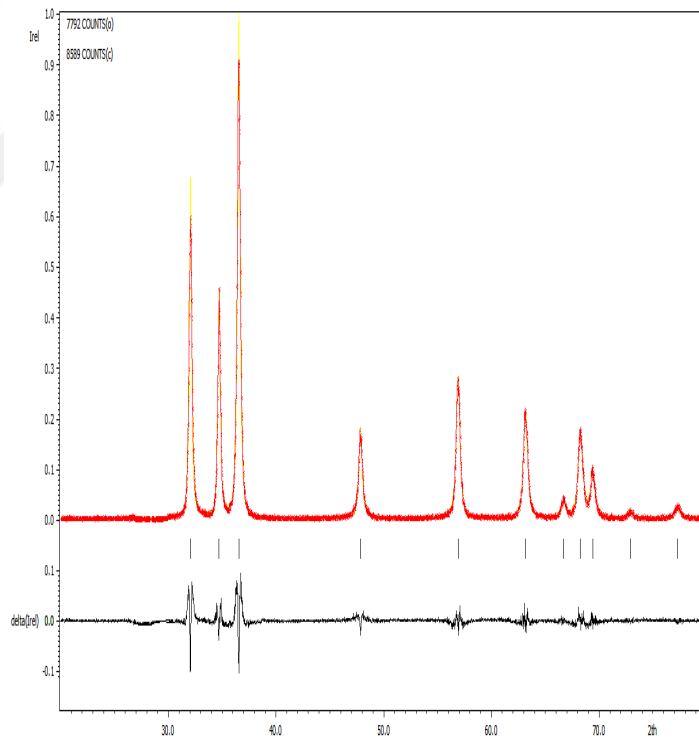
4.6 Preparation of $Zn_{1-x}Pr_xO$ nanoparticles by hydrothermal method ($x=0.01, 0.02, 0.03, 0.04, 0.05$)

4.6.1 XRD Study

The structural behavior of the $Zn_{1-x}Pr_xO$ ($x=0.01, 0.02, 0.03, 0.04, 0.05$) nanoparticles was determined by the XRD analysis in the range $30^\circ \leq 2\theta \leq 80^\circ$ degrees. All peaks positions were indexed and the second phase was not observed in all samples XRD patterns as shown in Fig.37. The XRD patterns catch out that all the sample synthesized at 1%, 2%, 3%, 4%, 5% Pr concentrations have hexagonal wurtzite structure along the (101) direction. Using XRD analysis of $Zn_{1-x}Pr_xO$ nanoparticle samples the concentration-dependent average nanorod sizes (D), lattice parameters, volume of the unit cell (V), and bond length (L) were determined and reported in table 4. Additionally, Rietveld analysis was shown for $Zn_{0.98}Pr_{0.02}O$ to qualify the sample in Fig.37. The goodness of fit (GOF): 3.28, expected profile (R_p): 14.54, and weighed profile (R_{wp}): 21.05 were calculated from the Rietveld analysis for $Zn_{0.91}Er_{0.09}O$. The cell parameters $a=b= 3.2462 \text{ \AA}$ and $c= 5.2719 \text{ \AA}$.



a)



b)

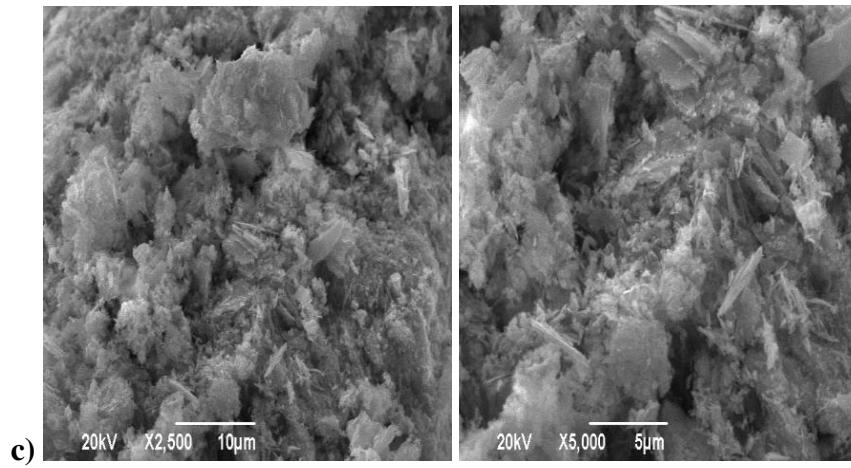
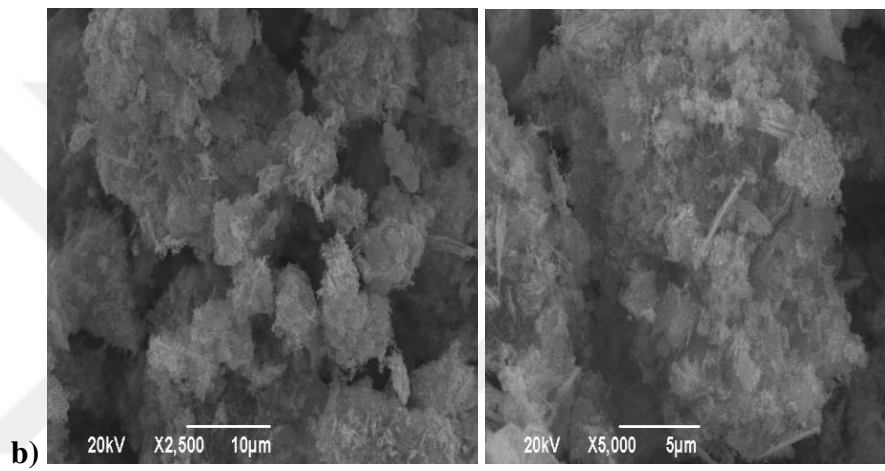
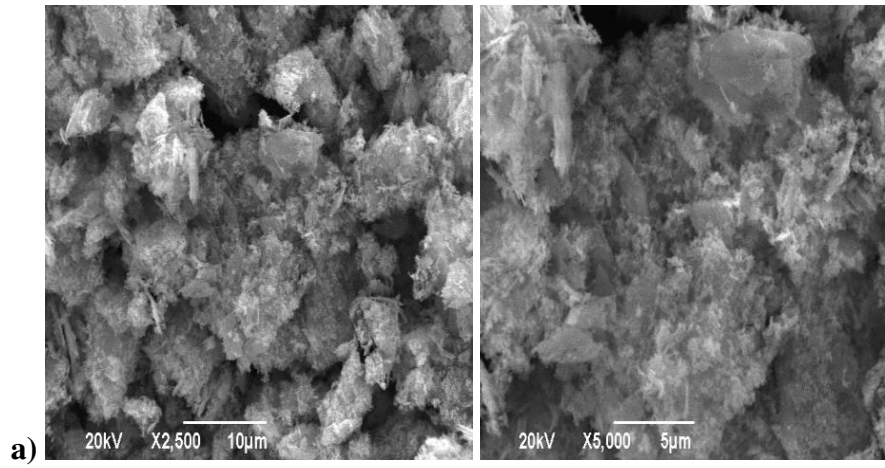
Figure 4.36 a) XRD patterns of $\text{Zn}_{1-x}\text{Pr}_x\text{O}$ ($x=0.01, 0.02, 0.03, 0.04, 0.05$) nanoparticles b) the XRD profile fitting from Rietveld analysis of $\text{Zn}_{0.98}\text{Pr}_{0.02}\text{O}$

Table 4.5 Cell parameters, atomic packing factor, average particle size, bond length, crystal lattice distortion degree and volume of the unit cell $Zn_{1-x}Pr_xO$ nanoparticles.

Sample Name	a (Å)	c(Å)	c/a	Grain size from XRD(nm)	L(ZnO)	R	V
$Zn_{0.99}Pr_{0.01}O$	3.214	5.156	1.604	22.21	1.987	1.017	46.12
$Zn_{0.98}Pr_{0.02}O$	3.220	5.164	1.603	21.39	1.993	1.018	46.36
$Zn_{0.97}Pr_{0.03}O$	3.218	5.162	1.604	20.44	1.989	1.018	46.28
$Zn_{0.96}Pr_{0.04}O$	3.219	5.162	1.603	22.73	1.990	1.018	46.31
$Zn_{0.95}Pr_{0.05}O$	3.212	5.152	1.603	17.81	1.986	1.018	46.02

4.6.2 SEM-EDS Study

The morphology of all $Zn_{1-x}Pr_xO$ ($x=0.01, 0.02, 0.03, 0.04, 0.05$) nanoparticles was studied by SEM technique by 10 and 5 μm magnifications. As seen in Fig.38 (a) to (e) the particle distribution is random and is dominated by particle agglomeration. The elemental composition of all samples was provided by the EDX analysis exhibited in Fig.39 (a) to (e). All peaks in EDX analysis belong to the extended composition without any other unwanted extra elemental peak contribution. The SEM image of the $Zn_{0.96}Pr_{0.04}O$ is shown that the particles are agglomerated and the shape of flower-like, and SEM image of (e) is observed of nano needle-like structure. In Figure 39 shows the EDX spectra that contain the Zn and O element, and trace amount of Pr element.



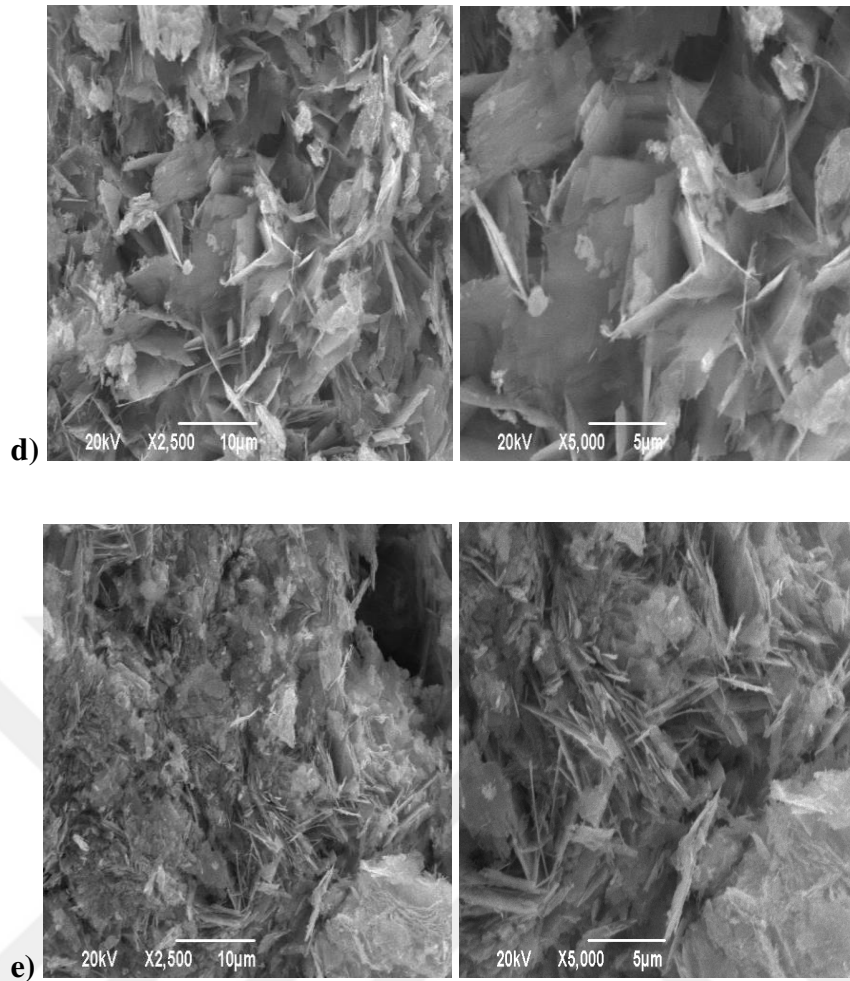
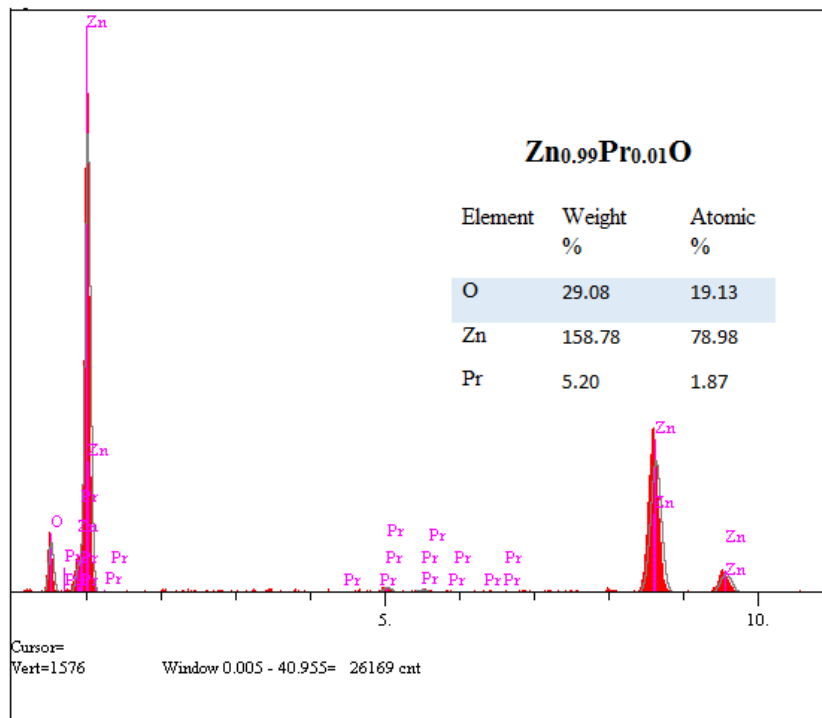
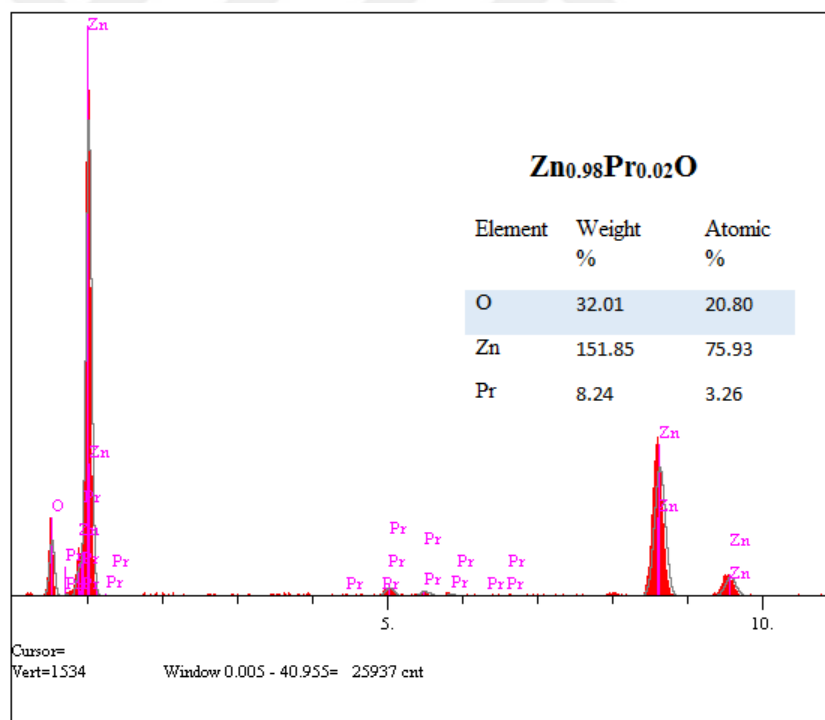


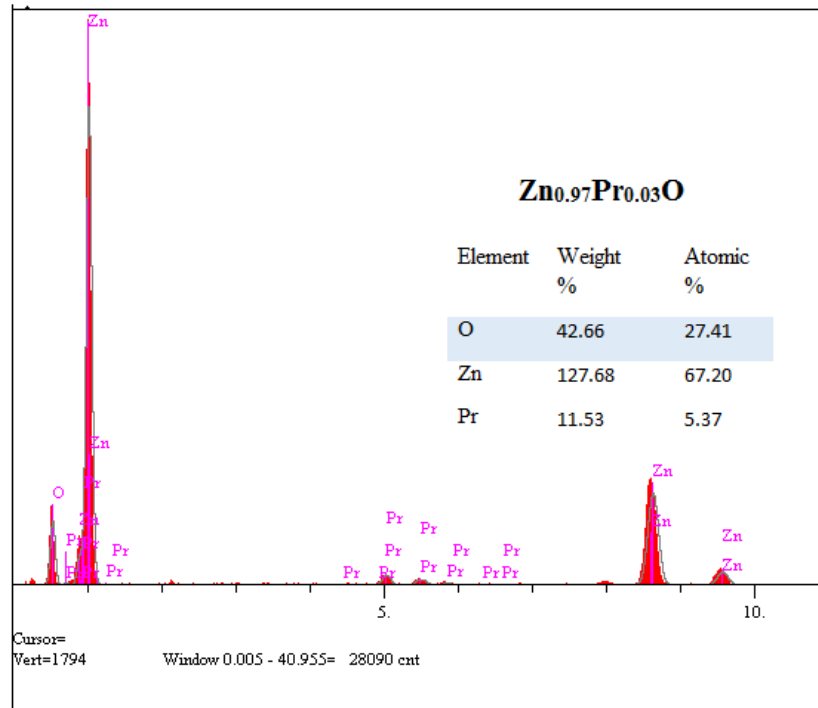
Figure 4.37 SEM images of 1%, 2%, 3%, 4%, 5% $Zn_{1-x}Pr_xO$ nanoparticles
 a) $Zn_{0.99}Pr_{0.01}O$ b) $Zn_{0.98}Pr_{0.02}O$ c) $Zn_{0.97}Pr_{0.03}O$ d) $Zn_{0.96}Pr_{0.04}O$
 e) $Zn_{0.95}Pr_{0.05}O$ respectively with 10 μm magnification and 5 μm magnification



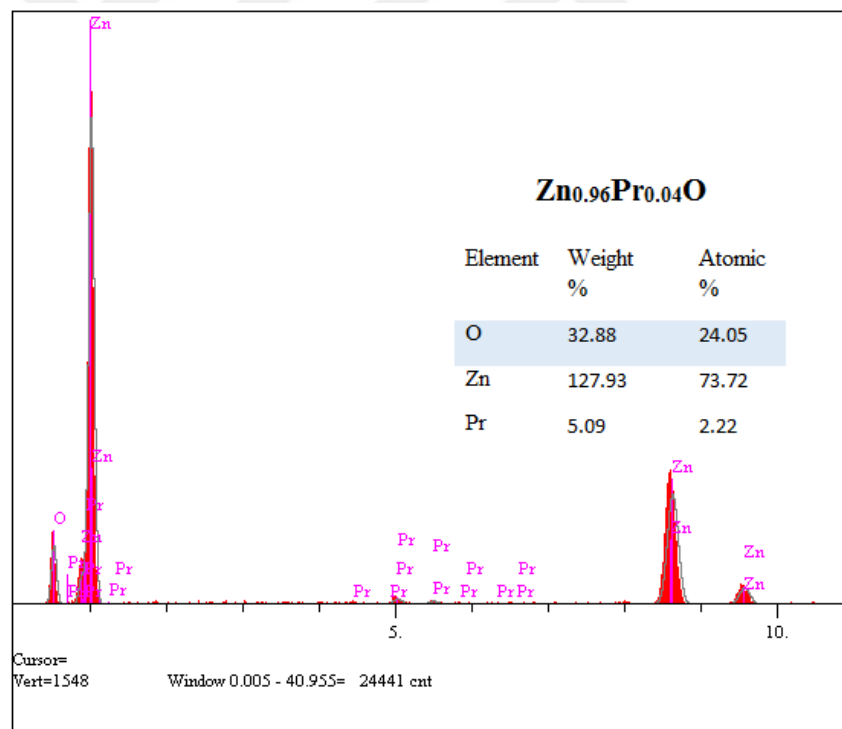
a)



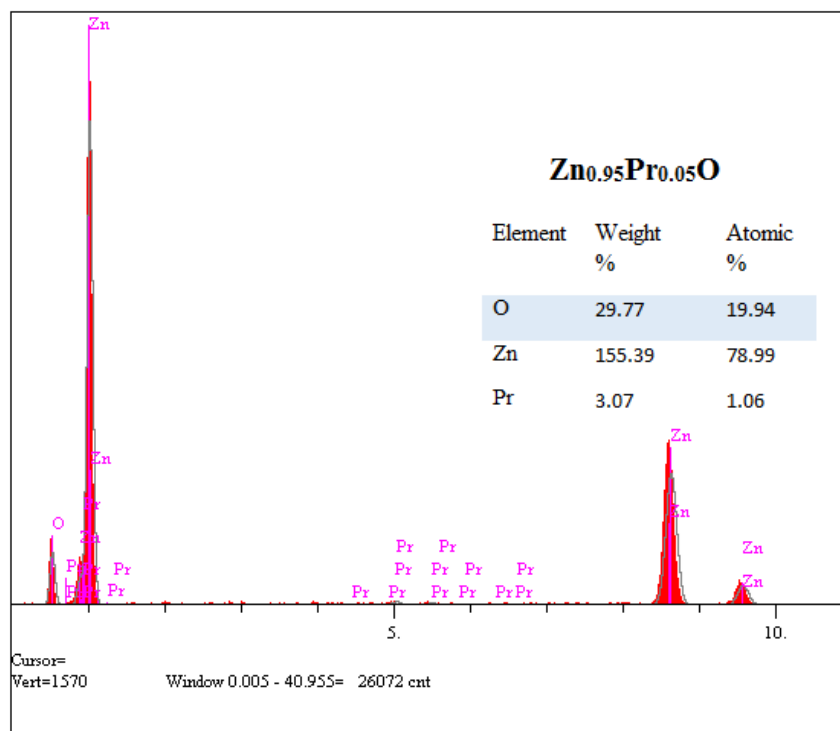
b)



c)



d)



e)

Figure 4.38 EDX image of the $Zn_{1-x}Pr_xO$ nanoparticles a) $Zn_{0.99}Pr_{0.01}O$ b) $Zn_{0.98}Pr_{0.02}O$ c) $Zn_{0.97}Pr_{0.03}O$ d) $Zn_{0.96}Pr_{0.04}O$ e) $Zn_{0.95}Pr_{0.05}O$ respectively

4.6.3 Optical Properties

The UV-visible diffuse reflectance of the $Zn_{1-x}Pr_xO$ nanoparticles were analyzed in the 300-700 nm range the optical properties and the result are plotted in Figure 40. As can be seen in the figure below, the Pr content increasing effect the all spectral regions. At 375 nm for 1 to 3 samples were observed sharp increases of reflectance, on the other hand for 4, and 5 Pr concentrations The optical absorption edge of Pr-doped ZnO nanoparticles shifted through the higher energy (blue shift) that is mean lower wavelength up to 4% Pr doping. However, the Pr concentration (5%) increasing was seen shift to lower energy (red shift) meaning higher wavelength. The blue shift of the reflectance can be explained with the Burstein-Moss effect that is known the phenomenon of widening of the band gap. According to these band gap energies, Pr doping based on the combining effect of the Burstein-Moss, strain and grain size.

The band gap energies of the samples can be calculated using the maxima of the $dR/d\lambda$ as a function of wavelength (figure 41). The band gap energy value is determined 3.229 eV for $Zn_{0.99}Pr_{0.01}O$, 3.240 eV for $Zn_{0.98}Pr_{0.02}O$, 3.239 eV for $Zn_{0.97}Pr_{0.03}O$, 3.244 eV for $Zn_{0.96}Pr_{0.04}O$, 3.234 eV for $Zn_{0.95}Pr_{0.05}O$ respectively.

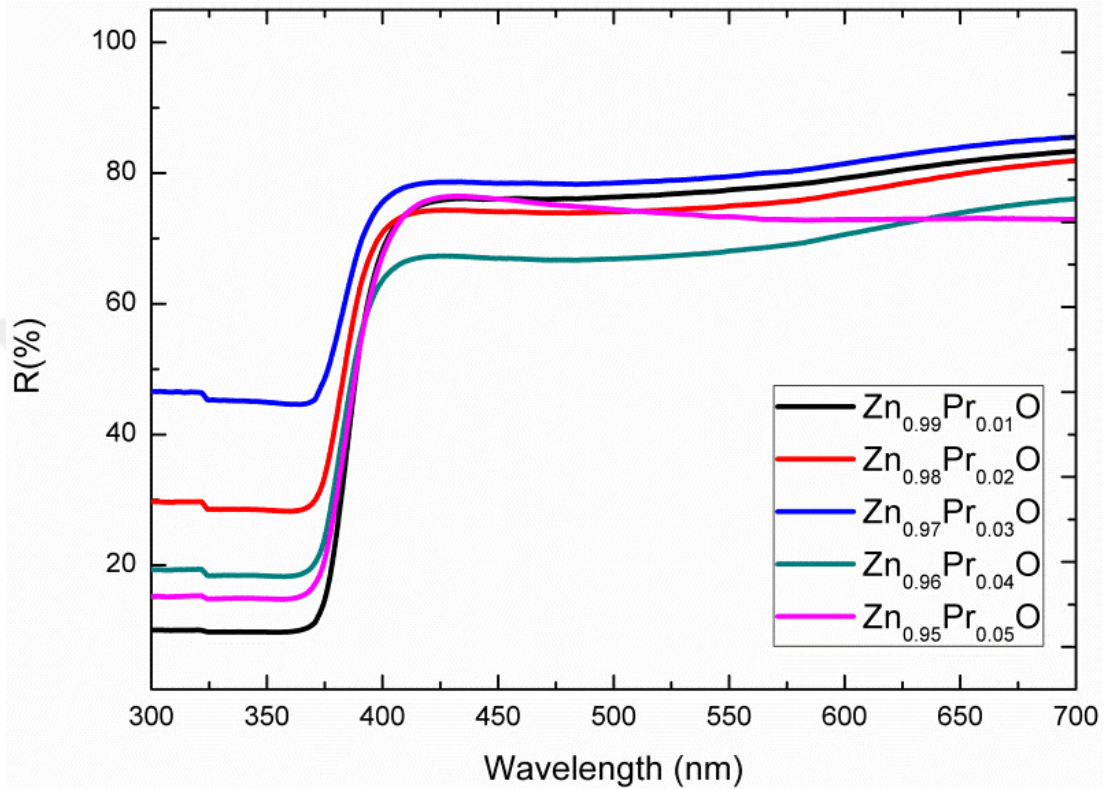


Figure 4.39 The reflectance of the $Zn_{1-x}Pr_xO$ ($x=0.01, 0.02, 0.03, 0.04, 0.05$) nanoparticles

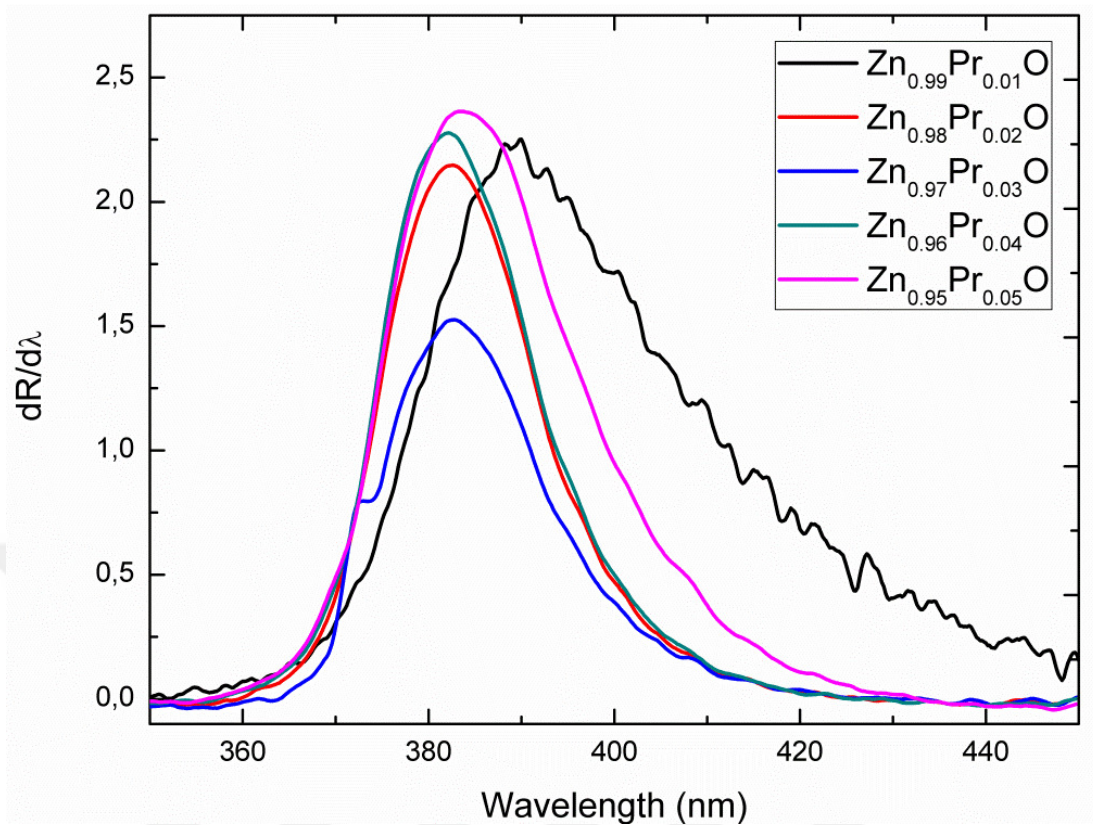


Figure 4.40 The plots of $dR/d\lambda$ as a function of wavelength for the $Zn_{1-x}Pr_xO$ ($x=0.01, 0.02, 0.03, 0.04, 0.05$) nanoparticles

5. CONCLUSIONS

In the first part of thesis, zinc oxide doped rare-earth elements (Er, Pr) were synthesized in different ratios using PET and glass substrates via hydrothermal method. Its structural and optical properties are analyzed based on their concentration dependence. ZnO doped Er thin films deposits on glass substrate signalized a stronger orientation of the crystallites belong (101) phase. ZnO doped Er PET substrate deposits showed a stronger orientation of the crystallites belong (002) phase. SEM analysis showed the change of the morphology of the samples with Er doping on glass substrate. Er, doping was caused spheroid-pyramidal like structure, rod-like structures, and obelisk-shaped nanorods images for higher doping levels. The optical measurements reveal that the absorption edge of the obtained films is observed to shift towards the lower wavelength (higher energy) region (blue shift) meaning there is a blue shift with increasing Er content (1%, 3%, 5%, %7).

According to XRD result of Er-doped ZnO on PET substrates exhibited as wurtzite structure depending on the increase in Er doping. Also, it was observed shift towards the big angle for the (002) peak direction with Er incorporation. As a result of this shift, it was concluded that Er atoms were effectively incorporated to the ZnO lattice because of the difference of ionic radius of Er^{+3} and Zn^{+2} . Er-doped PET samples were seen in different shapes according to increasing the concentration, the $\text{Zn}_{0.97}\text{Er}_{0.03}\text{O}$ cluster of grapes like structure, the $\text{Zn}_{0.95}\text{Er}_{0.05}\text{O}$ flower-like shaped, and $\text{Zn}_{0.93}\text{Er}_{0.07}\text{O}$, $\text{Zn}_{0.91}\text{Er}_{0.09}\text{O}$ have nanorods shaped. In the optical measurement part, blue shift (higher energy) was observed in the images of Er-doped ZnO films.

The second rare-earth element that is Praseodymium was doped on glass substrate. The XRD result shown (100), (002) peaks increases slowly. Thus the substitution of the Pr^{+3} ions cause to an expansion of the ZnO lattice along the a-axis, and c-axis. According to SEM analysis, they were seen flower-like and nanofiber-like structures. Additionally, optical results was shown that the blue shift to lower wavelength (higher energy).

In the last part of the thesis, the properties of the $Zn_{1-x}Er_xO$, and $Zn_{1-x}Pr_xO$ were studied that products obtained in powder form. Firstly, XRD patterns of the $Zn_{1-x}Er_xO$ nanoparticles showed that the orientation of (101) peaks in the structure. Hence, Er^{+3} ions lead to a bigger orientation along the c-axis. The small agglomeration on structure was observed by the SEM images. UV-VIS spectra results were explained the shift of the reflectance that decreases the concentrations observed blue shift to lower wavelength and increases the concentrations red shift to higher wavelength.

To examination of $Zn_{1-x}Pr_xO$ nanoparticles, the XRD results explained the enhanced peak intensities and the strongest peak of (101). No extra peaks are observed the meaning of that Pr^{+3} ions would precipitate out of ZnO lattice. In SEM analysis are clearly shown that the particles are agglomerated, and some of them own flower-like structure, and the other ones nano needle-like structure. The optical absorption edge of Pr-doped ZnO nanoparticles shifted through the higher energy up to 4% Pr-doping, however, 5% Pr-doped ZnO caused to shift to lower energy, it can be explained by the increase of concentration of Pr-doping.

6. REFERENCES

- Agrawal, Harshita, Kamendra Awasthi, Yogendra K Saraswat, and K Vibhav. 2017. "ZnO Nanoparticles Favours Heterogeneous Nucleation in PET – ZnO Nanocomposites." *Philosophical Magazine* 6435(May): 1–17. <http://dx.doi.org/10.1080/14786435.2015.1057254>.
- Anker, Gina M. 2012. "Case Studies in Medical-Surgical." 57: 625–30.
- Background, Historical et al. 2004. "Upconversion and Anti-Stokes Processes with f and d Ions in Solids."
- Baruah, Sunandan, and Joydeep Dutta. 2009. "Hydrothermal Growth of ZnO Nanostructures." *Science and Technology of Advanced Materials* 10(1).
- Behdadfar, Behshid et al. 2010. "History of Rietveld Analysis." *ACS Nano* 7(4): 284–88. <http://dx.doi.org/10.1016/j.cap.2009.06.007>
http://cdn.intechopen.com/pdfs/9730/InTech-Silver_nanoparticles_sensing_and_imaging_applications.pdf
<http://stacks.iop.org/0022-3727/43/i=47/a=474012?key=crossref.3028f161907e29eb045dbe673562dc85>
- Bhatia, Sonik, Neha Verma, and R K Bedi. 2016. "Optical Application of Er-Doped ZnO Nanoparticles for Photodegradation of Direct Red - 31 Dye." *Optical Materials* 62: 392–98. <http://dx.doi.org/10.1016/j.optmat.2016.10.013>.
- Brian, D et al. 2015. "Article Begins on next Page." 252(8): 1700–1710.
- Cagardová, Denisa, and Vladimír Lukeš. 2017. "Molecular Orbital Analysis of Selected Organic P-Type and n-Type Conducting Small Molecules." *Acta Chimica Slovaca* 10(1): 6–16.
- Caglar, Mujdat, Yasemin Caglar, and Saliha Ilcan. 2016. "Investigation of the Effect of Mg Doping for Improvements of Optical and Electrical Properties." *Physica B: Condensed Matter* 485: 6–13. <http://dx.doi.org/10.1016/j.physb.2015.12.049>.
- Carl R.(Rod) Nave. 2017. "HyperPhysics Concepts." <http://hyperphysics.phy-astr.gsu.edu/hbase/hph.html> (February 8, 2019).
- Chen, G Y et al. 2013. "Two-Color Upconversion in Rare-Earth-Ion-Doped Zr O 2 Nanocrystals." 163105(2006): 1–4.
- Conference, The Denver X-ray. 1972. "Conference Report." : 1972.
- cullity, B.D. 1978. "X-Ray Powder Diffraction (XRD)." 2nd ed. https://serc.carleton.edu/research_education/geochemsheets/techniques/XRD.html (February 9, 2019).

- Danckwerts, P.V. 2002. "Angewandte Chemie." *Chemical Engineering Science* 17(11): 955.
- Djurišić, Aleksandra B., and Yu Hang Leung. 2006. "Optical Properties of ZnO Nanostructures." *Small* 2(8–9): 944–61.
- Ebnesajjad, Sina, and Processible Fluoroplastics. 2003. "Semiconductor Materials Learn More about Semiconductor Materials Applications in Microelectronics In- Dustry Semiconductor Surface Chemistry."
- Faloon, D.B. "Pigments through the Ages - Technical Information - Zinc White." 1925. <http://www.webexhibits.org/pigments/indiv/technical/zincwhite.html> (February 8, 2019).
- Fan, Ranran, Fei Lu, and Kaikai Li. 2017. "Single-Mode Channel Waveguide at 1540 Nm in Er-Doped ZnO Thin Film." *Journal of Luminescence* 192(July): 410–13. <http://dx.doi.org/10.1016/j.jlumin.2017.07.003>.
- Garg, Ashish. "A Brief Introduction to Rietveld Analysis of XRD Patterns Powder Diffraction: The Rietveld Method and the Two Stage Method to Determine and Refine Crystal Structures from Powder Diffraction Data." https://www.iitk.ac.in/tkic/workshop/XRD/ppt/Prof Garg/AshishGarg_Rietveld.pdf.
- Heo, Sungeun et al. 2014. "Mole-Controlled Growth of Y-Doped ZnO Nanostructures by Hydrothermal Method." *Current Applied Physics* 14(11): 1576–81. <http://dx.doi.org/10.1016/j.cap.2014.09.008>.
- "JEOL - JSM-6390 - Scanning Electron Microscopes (SEM)□: HV/LV Tungsten/LaB6 SEMs - Scanning Electron Microscope by Jeol USA Inc." <https://www.environmental-expert.com/products/jeol-model-jsm-6390-scanning-electron-microscope-426298> (February 8, 2019).
- Jiang, Zhi Yuan et al. 2004. "Synthesis of Single-Crystalline ZnO Polyhedral Submicrometer-Sized Hollow Beads Using Laser-Assisted Growth with Ethanol Droplets as Soft Templates." *Advanced Materials* 16(11): 904–7.
- Kaur, Manpreet et al. 2018. "Structural, Morphological and Optical Properties of Eu-N Co-Doped Zinc Oxide Nanoparticles Synthesized Using Co-Precipitation Technique." *Vacuum* 155(May): 689–95. <https://doi.org/10.1016/j.vacuum.2018.06.046>.
- Kolodziejczak-Radzimska, Agnieszka, and Teofil Jesionowski. 2014. "Zinc Oxide- from Synthesis to Application: A Review." *Materials* 7(4): 2833–81.
- Lang, Jihui et al. 2016. "Synthesis and Photoluminescence Characterizations of the Er³⁺-Doped ZnO Nanosheets with Irregular Porous Microstructure." *Materials Science in Semiconductor Processing* 41: 32–37. <http://dx.doi.org/10.1016/j.mssp.2015.08.022>.

Law, Lambert-beer. "Vol. 14." 14.

Li, Hengda, Xinzhong Liu, and Zhigong Zheng. 2014. "Magnetic Behavior of Co-Mn Co-Doped ZnO Nanoparticles." *Journal of Magnetism and Magnetic Materials* 372: 37–40. <http://dx.doi.org/10.1016/j.jmmm.2014.07.006>.

Lin, Hang et al. 2010. "By Yb³⁺ in β -YF₃ Nanocrystals Embedded Transparent Glass Ceramics." 103511: 3–7.

Lop, D Q G Q U H H et al. 2015. "6Wuxfwxudo Dqg 2Swlfdo 3Urshuwlvh Ri 3U 'Rshg =Q2 Dqg 39\$ =Q 3U 2 1Dqrfprsvlwh)Uhh 6Wdqglqj)Lop." 9(1): 225–29.

McLeod, Saul. 2012. "Chapter 2: Experimental Methods." *Simply Psychology* 8: 15–64. <http://www.simplypsychology.org/experimental-method.html>.

Oxide, Magnesium, Titanium Dioxide, Zinc Sulfate, and Silicon Dioxide. 2016. "Zinc Oxide Learn More about Zinc Oxide Zinc Oxide Nanoparticles for Food Packaging Applications Advances in Agronomy Nanotechnology for Water Purification□: Applications of Nanotechnology Meth- Ods in Wastewater Treatment."

Pearsonhighered. 2013. "N-Type and P-Type Semiconductors." *Introduction to Semiconductors*: 1–13. <https://www.pearsonhighered.com/assets/samplechapter>.

Sakthivel, R. et al. 2017. "Effect of Post Annealing on Antibacterial Activity of ZnO Thin Films Prepared by Modified Silar Technique." *Oriental Journal of Chemistry* 33(1): 355–62.

de Sanctis, M., S. Pelletier, Y. Bienvenu, and M. Guigon. 1994. "On the Formation of Interfacial Carbides in a Carbon Fibre-Reinforced Aluminium Composite." *Carbon* 32(5): 925–30.

Senol, SD 2016. "Hydrothermal Derived Nanostructure Rare Earth (Er, Yb)-Doped ZnO: Structural, Optical and Electrical Properties." *Journal of Materials Science: Materials in Electronics* 27(8): 7767–75.

Senol, SD, A. Guler, C. Boyraz, and L. Arda. 2019. "Preparation Structure and Magnetic Properties of Mn-Doped ZnO Nanoparticles Prepared by Hydrothermal Method." *Journal of Superconductivity and Novel Magnetism*. <http://link.springer.com/10.1007/s10948-019-5030-7>.

Senol, Sevim D. et al. 2019. "Band Gap Engineering of Mg Doped ZnO Nanorods Prepared by a Hydrothermal Method." *Crystal Research and Technology* 54(3): 1–7.

Sreedharan, R Sreeja et al. 2016. "Influence of Pr Doping on the Structural , Morphological , Optical , Luminescent and Non-Linear Optical Properties of RF-Sputtered ZnO Films." 68(1): 341–50.

- Sze, SM., and Kwok Kwok Ng. 2007. *Physics of Semiconductor Devices*. Wiley-Interscience.
https://books.google.com.tr/books?hl=tr&lr=&id=o4unkmHBHb8C&oi=fnd&pg=PR7&dq=Sze+S.M.,+1969.+Physics+of+Semiconductor+Devices,+J.+Wiley%26+Sons,+52&ots=wGvifMBd61&sig=1NZYt9dWslF9NG1srIw9cPaZ1cA&redir_esc=y#v=onepage&q=Sze+S.M.%2C+1969.+Physics+of+Semiconductor+Devices%2C+J.+Wiley%26+Sons%2C+52&f=false (March 28, 2019).
- The editors of Encyclopaedia Britannica. 2019. “Zinc | Properties, Uses, & Facts | Britannica.Com.” *Jan 17*. <https://www.britannica.com/science/zinc> (February 8, 2019).
- Üzar, Neslihan. 2018. “Enhanced Optical and Electrical Properties of Y-Doped ZnO Nanoparticles Having Different Y Concentrations.” *Applied Physics A* 124(4): 1–6. <http://dx.doi.org/10.1007/s00339-018-1725-z>.
- Venkatachalam, Shanmugam et al. 2013. “Optoelectronic Properties of Nanostructured ZnO Thin Films Prepared on Glass and Transparent Flexible Clay Substrates by Hydrothermal Method.” *Japanese Journal of Applied Physics* 52(5 PART 2).
- Wang, Mao-hua, Zhong-yin Zhao, and Ting-ting Liu. 2015. “Synthesis of Pr-Doped ZnO Nanoparticles by Sol – Gel Method and Varistor Properties Study.” *JOURNAL OF ALLOYS AND COMPOUNDS* 621: 220–24. <http://dx.doi.org/10.1016/j.jallcom.2014.09.208>.
- Wang, Zhong Lin. 2004. “Zinc Oxide Nanostructures□: Growth , Properties and Applications.” 16: 829–58.
- Yu, Xiaochen et al. 2014. “Microstructure and Upconversion Luminescence in Ho 3 þ and Yb 3 þ Co-Doped ZnO Nanocrystalline Powders \$.” *Optics Communications* 313: 90–93. <http://dx.doi.org/10.1016/j.optcom.2013.09.071>.
- Zamiri, Reza, Avito Rebelo, Hamid Reza Bahari Poor, and J. M.F. Ferreira. 2014. “Quantum Cutting Effect and Photoluminescence Emission at about 1,000 Nm from Er–Yb Co-Doped ZnO Nanoplates Prepared by Wet Chemical Precipitation Method.” *Applied Physics A: Materials Science and Processing* 117(4): 2289–94.
- “Zinc Oxide | 1314-13-2.” https://www.chemicalbook.com/ChemicalProductProperty_EN_CB3853034.htm (February 8, 2019).
- Zou, Xiaoping et al. 2014. “Electrodeposition Combination with Hydrothermal Preparation of ZnO Films and Their Application in Dye-Sensitized Solar Cell.” *Journal of Chemistry* 2014(3): 1–6.



APPENDICES

7. APPENDICES

7.1 Appendix A XRD data of samples

Table A.1. 2θ , d and hkl values of $Zn_{1-x}Er_xO$ ($x= 0.03, 0.05, 0.07, 0.09$) thin films on glass substrates.

Sample name	2θ	d_{values}	hkl
Zn_{0.97}Er_{0.03}O	32.260	2.7726	100
	34.900	2.5687	002
	36.720	2.4454	101
Zn_{0.95}Er_{0.05}O	32.520	2.7510	100
	35.080	2.5559	002
	36.920	2.4327	101
Zn_{0.93}Er_{0.07}O	32.380	2.7626	100
	35.040	2.5587	002
	36.860	2.4365	101
Zn_{0.91}Er_{0.09}O	32.240	2.7743	100
	34.940	2.5658	002
	36.720	2.4454	101

Table A.2. The 2θ , d , and hkl values of $Zn_{1-x}Er_xO$ ($x=0.03, 0.05, 0.07, 0.09$) films on PET substrate

Sample name	2θ	d_{values}	hkl
Zn_{0.97}Er_{0.03}O	31.880	2.8048	100
	34.520	2.5961	002
	36.360	2.4688	101
Zn_{0.95}Er_{0.05}O	32.000	2.7945	100
	34.680	2.5845	002
	36.500	2.4597	101
Zn_{0.93}Er_{0.07}O	31.580	2.8307	100
	34.520	2.5961	002
	36.260	2.4754	101
Zn_{0.91}Er_{0.09}O	31.720	2.8186	100
	34.360	2.6078	002
	36.180	2.4807	101

Table A.3. The 2θ , d and hkl values of $Zn_{1-x}Pr_xO$ films on glass substrate ($x=0.01, 0.02, 0.03, 0.04, 0.05$)

Sample name	2θ	d_{values}	hkl
Zn_{0.99}Pr_{0.01}O	32.360	2.7643	100
	35.020	2.5602	002
	36.840	2.4378	101
Zn_{0.98}Pr_{0.02}O	32.340	2.7659	100
	34.980	2.5630	002
	36.860	2.4365	101
Zn_{0.97}Pr_{0.03}O	31.460	2.8413	100
	34.140	2.6241	002
	35.940	2.4967	101
Zn_{0.96}Pr_{0.04}O	32.400	2.7610	100
	35.040	2.5587	002
	36.880	2.4352	101
Zn_{0.95}Pr_{0.05}O	32.320	2.7676	100
	34.980	2.5630	002
	36.820	2.4390	101

Table A.4. The 2θ , d and hkl values of $Zn_{1-x}Er_xO$ nanoparticles ($x=0.03, 0.05, 0.07, 0.09$)

Sample name	2θ	d_{values}	hkl
Zn_{0.97}Er_{0.03}O	31.886	2.8043	100
	34.546	2.5942	002
	36.352	2.4693	101
Zn_{0.95}Er_{0.05}O	31.774	2.8139	100
	34.434	2.6024	002
	36.268	2.4749	101
Zn_{0.93}Er_{0.07}O	31.816	2.8103	100
	34.448	2.6013	002
	36.296	2.4730	101
Zn_{0.91}Er_{0.09}O	31.844	2.8079	100
	34.476	2.5993	002
	36.310	2.4721	101

Table A.5. The 2θ , d and hkl values of $Zn_{1-x}Pr_xO$ nanoparticles ($x=0.01, 0.02, 0.03, 0.04, 0.05$)

Sample Name	2θ	d_{values}	hkl
Zn_{0.99}Pr_{0.01}O	32.120	2.7844	100
	34.760	2.5787	002
	36.600	2.4532	101
Zn_{0.98}Pr_{0.02}O	32.080	2.7887	100
	34.720	2.5816	002
	36.560	2.4558	101
Zn_{0.97}Pr_{0.03}O	32.080	2.7878	100
	34.720	2.5816	002
	36.560	2.4558	101
Zn_{0.96}Pr_{0.04}O	32.080	2.7878	100
	34.740	2.5802	002
	36.580	2.4545	101
Zn_{0.95}Pr_{0.05}O	32.180	2.7793	100
	34.780	2.5773	002
	36.620	2.4519	101

8. CURRICULUM VITAE

Name Surname: Melike İMAMOĞLU

Place and Date of Birth: İstanbul, January 1992

University: Bolu Abant İzzet Baysal University

Bachelor's Degree : 2.56/4

MSc Degree : 3.50/4

Email: melikeimamoglu@gmail.com